Dissertations and Theses

7-11-2014

Axial Compressor Design with Counter-Rotation and Variable RPM for Stall Mitigation

Madhur Tiwari
Embry-Riddle Aeronautical University - Daytona Beach

Follow this and additional works at: https://commons.erau.edu/edt

Part of the Aerospace Engineering Commons

Axial Compressor Design with Counter-Rotation and Variable RPM for Stall Mitigation

MASTER OF SCIENCE THESIS

For obtaining the degree of Master of Science in Aerospace Engineering at Embry-Riddle Aeronautical University

Madhur Tiwari

July 11th, 2014

Department of Aerospace Engineering   ·   Embry-Riddle Aeronautical University

EMBRY–RIDDLE AERONAUTICAL UNIVERSITY
DEPARTMENT OF
AEROSPACE ENGINEERING

This thesis entitled "**Axial Compressor Design with Counter-Rotation and Variable RPM for Stall Mitigation**" by **Madhur Tiwari** was prepared under the direction of the candidate's thesis committee chairman, Dr. Magdy Attia, Department of Aerospace Engineering, and has been approved by the members of his thesis committee. It was submitted to the Aerospace Engineering Department and was accepted in partial fulfillment of the requirements for the degree of **Master of Science** in Aerospace Engineering.

THESIS COMMITTEE:

Dr. Magdy Attia
Chairman

Dr. Mark Ricklick
Member
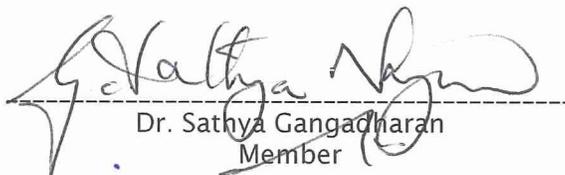
Dr. Sathya Gangadharan
Member

Dr. Yi Zhao,
Graduate Program Coordinator

7/21/14
Date
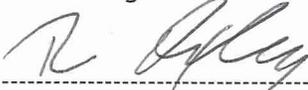
Dr. Robert Oxley,
Associate Provost

7-21-14
Date

3

Contents

List of Tables

List of Figures

Nomenclature

A   Area(m2)

BP   Bypass

BPR   Bypass Ratio

C.C   Combustion Chamber

CFD   Computational Fluid Dynamics

DF   Diffusion Factor

h   Enthalpy(J/Kg)

H/T   Hub to Tip Ratio

HDBPE   High Double Bypass Engine

HP   High Pressure

HPC   High Pressure Compressor

HPT   High Pressure Turbine

IGV   Inlet Guide Vane

IPC   Intermediate Pressure Compressor

IPT   Intermediate Pressure Turbine

LP   Low Pressure

LPC   Low Pressure Compressor

LPT   Low Pressure Turbine

M   Mach Number

NPSS   Numerical Propulsion Simulation System

OBPR   Overall Bypass Ratio

OGV   Outlet Guide Vane

P   Pressure(Pa)

Pri   Primary

R   Gas Constant(J/Kg.K)

RPM   Revolutions per Minute

S   Entropy(J/Kg.K)

Sec   Secondary

Greek Symbols

Δ Change

Π Stage Pressure Ratio

α Absolute Flow Angle(deg.)

β Relative Flow Angle(deg.)

γ Specific Heat Ratio

η Efficiency

λ Work Coefficient

ξ Stator Loss Coefficient

ρ Density(Kg/m3)

σ Solidity

Φ Flow Coefficient

Acknowledgement

I would like to express my sincere gratitude to Dr. Attia. His skills and knowledge not only helped me through my research but encouraged me to push forward in the field of Aerospace Engineering. I would also like to thank Dr. Mark Ricklick and Dr. Sathya Gangadharan for their support with this research paper.

Dedicated to my Mother and Kanika.

Abstract

Compressor Stall, an aerodynamic instability due to abnormal air flow in the compressor resulting in loss of total pressure and compressor performance. One of the reasons of compressor stall is due to rise in static back pressure at compressor exit which may result from an imbalance of incidence angle at the rotor and stator and rotational speed. The paper presents the results of a new axial compressor design with counter rotation and variable RPM. Counter-Rotation is used to push compressor performance during stall by moving the operating point away from surge line with a higher pressure ratio rise. Initially an axial compressor is designed with counter-rotation at design point. The flow is modelled by means of Navier-Stokes computation using the upstream rotor conditions and exit static pressure condition with k-epsilon as the turbulence model. Compressor exit conditions are then changed to stall the compressor. After the compressor stalls the RPM of the counter-rotating stage is varied until the compressor recovers from the stall. This novel idea unlike the conventional stall control systems mitigates the stall without compromising compressor performance, in fact it helps to increase the performance and pressure ratio of the compressor with the means of counter-rotation and variable RPM.

Chapter 1

Introduction

1.1 Background

Compressors date back as early as 1884 when Sir Charles Parsons obtained a patent in the form of *reversed turbine* which is as old as the reaction turbine itself. However, reversing the turbine for usage as a compressor was found to have overall efficiency of less than 40%. Parsons later on built many of these machines based on reversing the turbine. These machines were later able to achieve efficiency of about 55% and the reason for this low efficiency was attributed to blade stall. Later, he worked on two-stage axial compressor which was abandoned because it proved to be unstable, assumed to be caused by compressor surge.

In 1926, A.A Griffith started working on the theory of airfoil design for compressors and turbines in a gas turbine engine. Until then no work was done in this area due to mechanical and design limitations. Alongside with Griffith, the theory of axial compressor and its development is linked to Cox (1946) and Constant (1945). The work of Griffith's team at Royal Aircraft Establishment concluded that high efficiency of 90% is attainable using small stage axial compressor i.e. low pressure ratio.

The difficulty associated with the development of the axial compressor is the decelerating flow, as opposed to accelerating it in the turbine. Decelerating the flow in compressors results in adverse pressure gradient, which causes stall and sometimes total loss in pressure causing compressor to surge. This led to the development of multi-stage axial compressor design where the rise in total pressure is achieved via multiple rotor-stator combinations, called stages, to avoid stall.

Developments in compressor design have been ongoing since the time they were invented. Various types of control systems and designs are developed by companies like GE, Rolls-Royce etc. to achieve better efficiency and to improve stability in the engine.

1.2 Theory

1.2.1 Axial Compressor

An axial compressor is a component of various industrial and aircraft gas turbines where flow enters and exits axially flowing parallel to the axis of rotation. An axial compressor works by accelerating the flow and then diffusing it to obtain a rise in total pressure. Axial compressors are comprised of multiple stages of rotor and stator combinations. The rotor adds work to the air and accelerates the flow and the stator diffuses the flow and converts the gain in work to pressure rise. Compressors consist of various stages: 1) Rotor and Stator make up a stage, 2) An inlet guide vane (IGV) is placed at the compressor inlet to impart swirl to the upstream flow and to change the flow requirement in the compressor, 3) Sometimes an Exit Guide Vane is also placed at the compressor exit to align the flow in the direction parallel to the axis of rotation.

Axial flow compressors work by incrementally increasing pressure stage by stage. Axial compressors are efficient and the table below shows the recent pressure ratio achieved by industrial, aerospace and research application.

Table 1.1 Different types of gas turbine engines and applications

Type of Applications	Type of Flow	Inlet Relative Mach Number	Pressure Ratio per Stage	Efficiency per Stage
Industrial	Subsonic	0.4-0.8	1.05-1.2	88%-92%
Aerospace	Transonic	0.7-1.1	1.15-1.6	80%-85%
Research	Supersonic	1.05-2.5	1.8-2.2	75%-85%

There has been considerable growth in gas turbine engines over the last few decades. The advancements in higher pressure ratios, stall control systems, and materials have resulted in very efficient and high thrust producing jet engines. The Table above shows the engine pressure ratio development trend since the invention of gas turbines.

1.2.2 Stall and Surge

There are various types of aerodynamic and mechanical instabilities that arise in an axial compressor, however stall and surge are the most common and can be catastrophic for a gas turbine engine.

There are three types of compressor stall that can occur in an engine:

1. Individual Blade Stall

   This type of stall occurs when all the blades in a compressor stall altogether without any propagation mechanism. The cause of this occurrence is currently unknown. However, mechanical design and manufacturing defects are presumed causes.

2. Rotating Stall

This type of stall was observed by Whittle and his team on a centrifugal compressor system. Rotating stall is comprised of zones of stalled air flow which propagate opposite to the direction of rotation. This type of stall is the most common type of stall occurrence. The Figure 1.1 below shows the propagation of stall in a blade row (blade 2). Due to flow perturbation, blade #2 is stalled before the other blades and fails to produce sufficient pressure rise to maintain the flow. The decelerated flow around the blade diverts, which increases the incidence angle of attack on blade 3. Due to the rise in incidence angle, blade #3 might stall next, which usually causes a chain reaction and stalls all the blades in the row causing the stage to fail. If left untreated this stalled stage can induce compressor surge, where there is a complete backflow of the air and engine failure might occur.
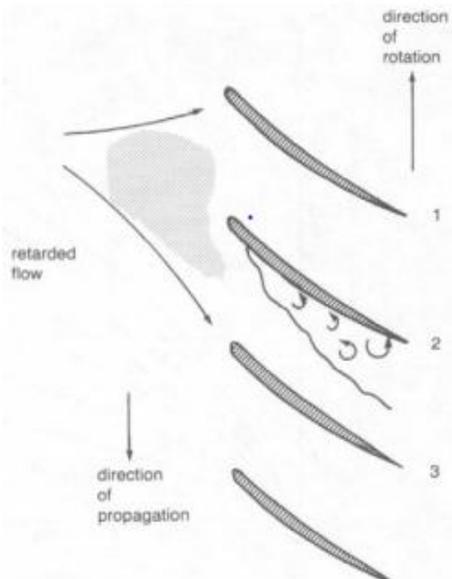
Fig 1.1 Stall in a Blade Cascade

3. Stall Flutter

This phenomenon occurs due to the stalling of the flow around the blade. Stall flutter induces Karman vortices in the airfoil wake. Whenever the frequency of the vortices matches the natural frequency of the airfoil, flutter will occur which can cause blade to fail. The Figure below shows flutter regions on a compressor map of a transonic compressor.
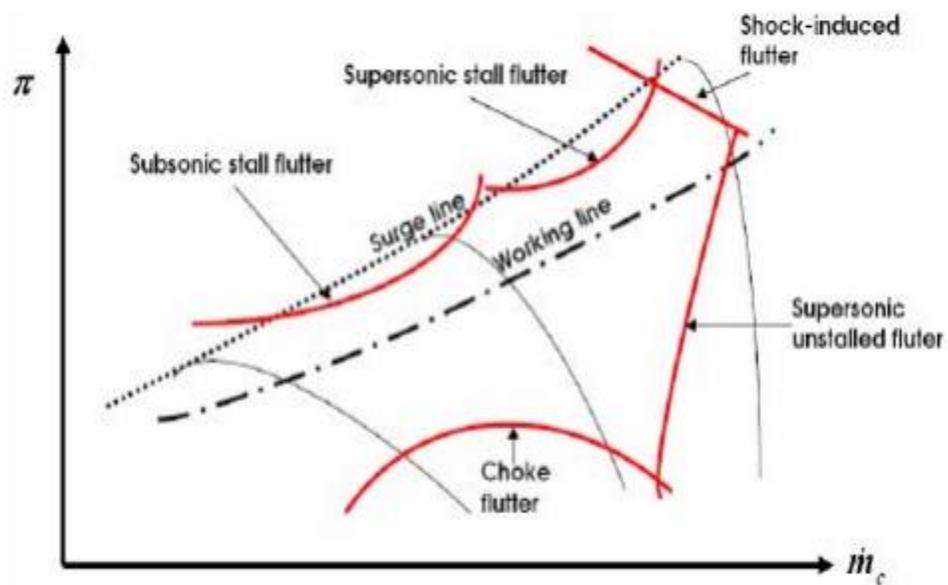
Fig 1.2 Compressor Map [Ref. GasTurb 11.0 Manual]

1.2.3 Stall Control Methods

Various methods have been devised to control and eliminate stall in an axial compressor. Stall control systems can be distinctively divided into two parts: Active stall control and passive stall control systems.

1. Active Stall Control System:

   In this type of system, compressor stall is avoided or eliminated by dynamically changing compressor characteristics like flow inlet angle. One example of this type of system is a variable IGV, which reduces relative incidence angle of the flow at the rotor inlet. Bleed valves at compressor exit is also an example of active stall control system, which reduces the increase in back pressure at the time of stall to reduce the risk of compressor back flow and surge, this type of stall control was developed by NASA Glenn Research.

   NASA Glenn Research is currently working on novel system to control stall which falls in the category of Active Stall Control system which is known as compressor stall control through end wall recirculation. In this research End wall recirculation is implemented by bleeding the air from the casing of the axial compressor at the last stage. Bleed ports are circumferentially installed over the casing and they occupy only 20% of the total circumference. This type of active stall control system increases the reliability of transonic compressor systems. However, it must be noted here that bleeding out air to alleviate stall causes the compressor to underperform due to pressure loss.

2. Passive Stall Control System:

This type of compressor stall recovery system is where stall control measures are pre-installed to avoid stall in the compressor. For Example: passages designed in a gas-turbine engine for the flow are kept at low turning angles to avoid recirculation.

Currently there is lot of research being done passive stall control system since install passive control system is cheaper and more reliable as it acts as a stall "prevention" method unlike the active stall control system which takes places only after the compressor has been stall. One of the examples of the passive stall control system can be seen in a turbine blade to avoid horse shoe vortex. Here a "cow-catcher" design and re-adjustment of the velocity triangles is done to avoid the formation of vortices to loss in momentum of the flow the at the end walls of a blade. This type of correction in blade significantly improves the performance of the turbines.

Another good example of a passive control system is a flow separator in an axial compressor. The flow separator was developed by General Electric engineers to remove foreign matter such as sand, dust and water from the air stream supplied to the compressor. However, the secondary role of a flow separator is avoid stall due foreign matter which can cause boundary layer separation and can cause the compressor to stall.

1.2.4 Counter-Rotation

In a traditional gas turbine engine, the compressor consists of rotors moving in the same direction attached to a shaft. Counter-rotation on the other hand is a concept where rotors sequentially move in opposite direction to each other, thus producing higher pressure and reducing the length and weight of the engine. The RPM of stages are different which gives higher degree of freedom in designing the compressor. However, counter-rotation results in higher tip relative Mach number which limits its design. Also, the reason counter-rotation is not seen in today's compressors is because of the mechanical complexities. The figure below shows a typical counter-rotating arrangement.
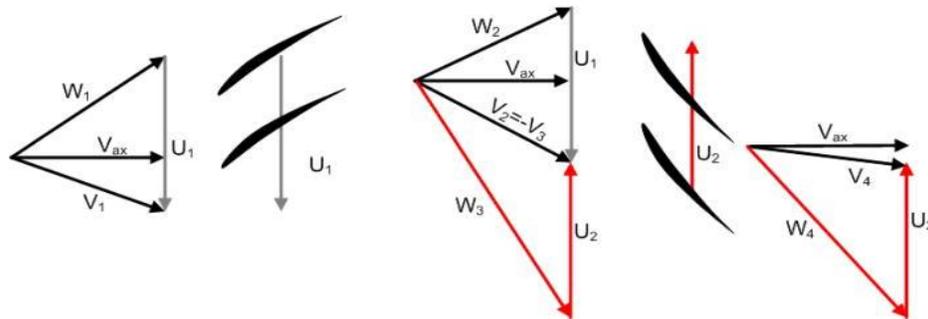
Fig 2.4: Counter-Rotating rotor blades

Various designs have been made using counter-rotating compressor system however none them have been used for stall control. A research done by MIT in 2006 showed successful increase in pressure by 50% than a conventional compressor system. However, the rotor were aspirated in that case to prevent the stall. This type of stall control using aspirated blades falls in passive stall control category.

Chapter 2

Setup and Methodology

2.1 Introduction

A counter-rotating compressor was designed by implementing a mean line analysis in EXCEL which was then simulated using ANSYS CFX. Preliminary design was done using EXCEL, all the design parameters for the compressor were kept within the aerodynamic, thermodynamic and structural limits. After the design parameters were fixed, the geometric points for the compressor were transferred to ANSYS Bladegen. Meshing was done using Turbogrid, after the mesh completion the compressor was set up in CFX for simulation. Design parameters from EXCEL were taken for inlet total pressure, RPM and outlet static pressure. For analysis, the simulation was divided into three parts: 1) Simulation of 2-Stage Counter-Rotating compressor at design point, 2) Simulation of 2-Stage Counter-Rotating compressor at stall, 3) Stall recovery simulation by varying RPM of stalled compressor. Compressor was stalled by incrementally increasing the outlet static pressure.

Variable RPM design is chosen to be an active stall control system in this research. In an axial compressor system, stall and surge initiates usually at the last few stages of the compressor, if left uncontrolled it can cause compressor failure. This problem can be fixed by re-energizing the flow by increasing the mass flow and velocity which re-attaches the separated boundary layer. However, by changing the RPM in a conventional one spool compressor causes the stall to become worse due increase in Mach relative number for end stages. This problem is fixed by splitting the compressor in two parts and making a dual spool compressor where the two spools are rotating in different direction causing the rotors to counter-rotate with each other. To find the best solution for getting

the RPM to fix the stall, an iterative process was used. After simulating stall conditions by increasing the static back pressure the RPM was slowly varied from 18000 to 21000 in steps of 500 and after simulating various times it was found out that the RPM of 21000 was the minimum RPM that was required to fix the stall in the compressor.

The Figure below shows the compressor setup that was used to design and run the simulation. As it can be seen, Rotor 1 rotates in clockwise direction with RPM of 18000 which is followed by the stator to reduce inlet incidence angle at Rotor 2 inlet. Rotor 2 rotates in anti-clockwise (opposite to Rotor 1) with RPM of 18000 at design point. It must be noted that both rotors are assumed to have the ability to rotate at different RPM values at off-design conditions.
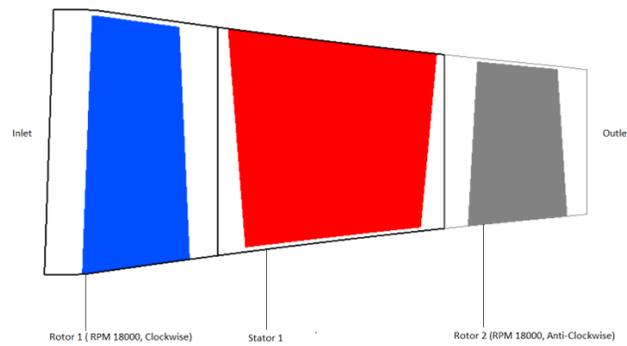
Fig 2.5: Compressor Setup

The following process gives a visual summary of the design steps which were taken into account. The process was repeated for various boundary conditions by changing the outlet static pressure until the compressor stalled. After the compressor stalled, the RPM was adjusted in the 2nd compressor stage to recover the compressor from stall.
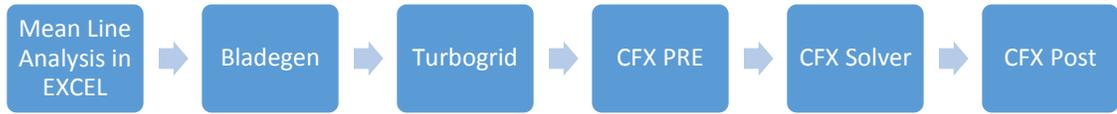
Fig 2.1 Design Setup and Process

2.2 Design Setup

2.2.1 EXCEL

The preliminary mean line design was done using EXCEL for the compressor. The following table lists the inlet conditions for the compressor. A low-pressure compressor is assumed upstream of the high-pressure compressor.

Table 2.1: Design Parameters at Inlet Point

Pressure Ratio	2.5
RPM Rotor 1	18000
RPM Rotor 2	18000
Inlet Mach	0.4
Mass Flow	50 (Kg/s)
Inlet Pressure (Static)	303975 (Pa)
Inlet Temperature (Static)	473 (K)
Gamma	1.4
Gas Constant (R)	287 (J/Kg-K)
Hub to Tip Ratio	0.72
Inlet Air Flow Angle	0° (Axial Flow)
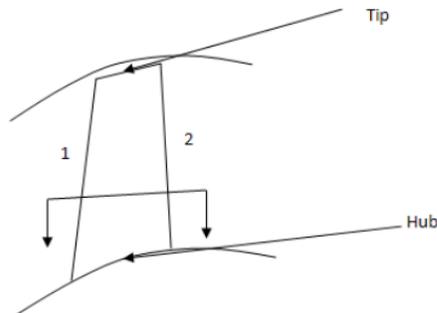
Fig 2.1 Meridional View of a Typical Compressor Rotor
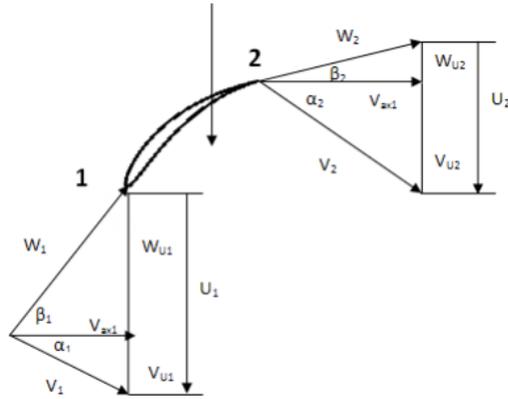
Fig 2.3: Velocity Triangles of a Typical Compressor Rotor Blade

Using the design conditions from the table above the high pressure compressor was designed. Free vortex radial equilibrium was taken into account and Euler-Turbomachinary equations were used for velocity triangle calculations at mid-span.

The equation below is the free vortex radial equilibrium equation in terms of radius and circumferential velocity. It was used to calculate circumferential velocity at the hub and tip of the blade given the velocity and radius at mid-span

$$r.V_u = K$$

Euler-Turbomachinary equation was used to calculate circumferential velocity components at the exit of the rotor for the mid-span.

$$\Delta h_o = U_2 V_{U_2} - U_1 V_{U_1}$$

Diffusion Factor: The diffusion factor (DF), a measure of blade loading, is a non-dimensional number used to ensure that flow separation across the airfoil does not occur thus preventing stall. The upper limit for the diffusion factor was taken to be 0.5. The diffusion factor can be given by:

$$DF = 1 - \frac{W_{ex}}{W_{in}} + \frac{W_{in} - W_{ex}}{2.\sigma.W_{in}} \qquad (2.1)$$

Flow Coefficient: The flow coefficient (ϕ) is the ratio of the axial velocity to the circumferential velocity. This is a characteristic for the mass flow behavior through the stage. The upper value of the flow coefficient was taken to be 0.75. The flow coefficient can be given by:

$$\phi = \frac{V_{ax_{exit}}}{U_{exit}}$$

2.2.2 Computational Fluid Dynamics (CFD) Modelling

CFD was done using CFX, which is part of the ANSYS suite of software programs. After the preliminary design completion in EXCEL, the co-ordinates were imported to Bladegen for stage design. The process is as follows:

2.2.2.1 Bladegen

EXCEL co-ordinates were imported in MM for better visualization in Bladegen working window. Normal layer thicknesses for the blades were optimized after analyzing several CFD simulations. For the initial run, generic blade thickness trend was used across the chord of the blade. The thickness was then optimized for a better Mach profile.

The Following table shows the bladegen step for the Rotor 1 at the hub. It can be seen that change in beta for the rotor is low ($\approx 16°$). Therefore, the work done by the rotor is largely due to its high RPM. It must be noted that the blades are supersonic in nature. It must also be noted here that for the CFD analysis of the blade sections are divided into three layers i.e. hub, mid and tip.

The following parameters were taken from mean line analysis for bladegen modelling.

Table 2.2: Bladegen input parameters

Parameters	Rotor 1	Stator 1	Rotor 2
Inlet Radius (hub) (MM)	212.462000	218.666000	225.792000
Exit Radius (hub)(MM)	216.739000	224.742000	228.957000
Inlet Radius (tip)(MM)	287.378000	282.182000	274.119000
Exit Radius (tip)(MM)	284.046000	275.271000	271.266000
Number of Blades	28	36	38
Inlet Beta (Degrees) (HUB)	66.168	43.187	64.510
Outlet Beta (Degrees)(HUB)	50.410	4.833	51.800
Inlet Beta (Degrees) (TIP)	72.357	36.062	68.390
Outlet Beta (Degrees)(TIP)	63.890	3.965	56.280
Machine Type	Axial Compressor	Axial Compressor	Axial Compressor

Normal thickness calculations for the blades were done using an iterative process. A generic parabolic thickness trend was chosen at first and multiple simulations were analyzed to get the correct shock placement over the airfoil. Also, the thickness curve is of utmost importance for getting the correct inlet and outlet angles for the airfoil.

The following figures show the bladegen setup at the hub for Rotor 1, Stator 1 and Rotor 2. See Appendix for tip and mid.
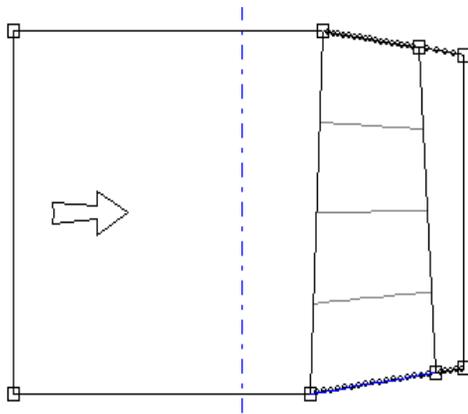
Fig 2.6: Meridional View for Rotor 1 at hub
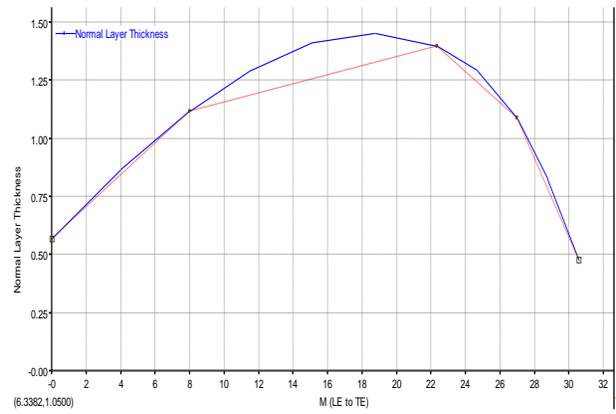
Fig 2.7: Normal Thickness trend for rotor 1 at hub
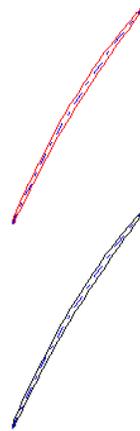
Fig 2.8: Blade Passage for rotor 1 at hub
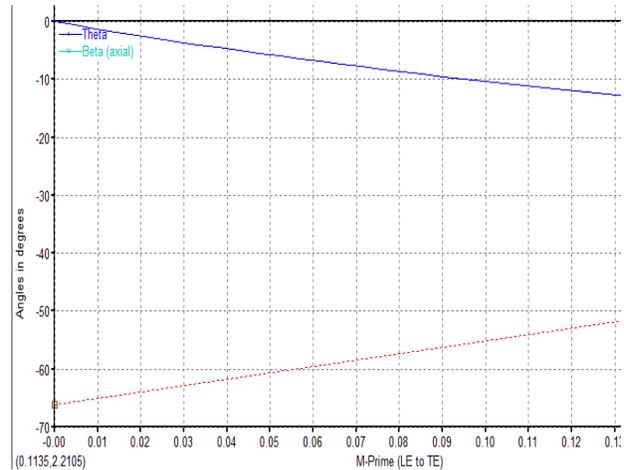
Fig 2.9: Beta over the airfoil for rotor 1 at hub
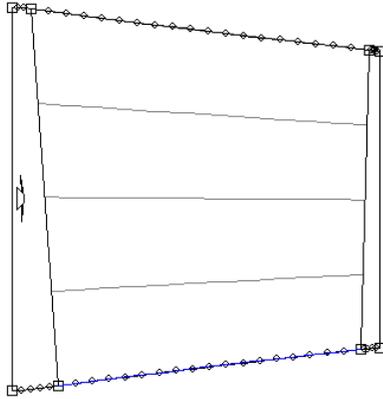
Fig 2.10: Meridional View for Stator 1 at hub
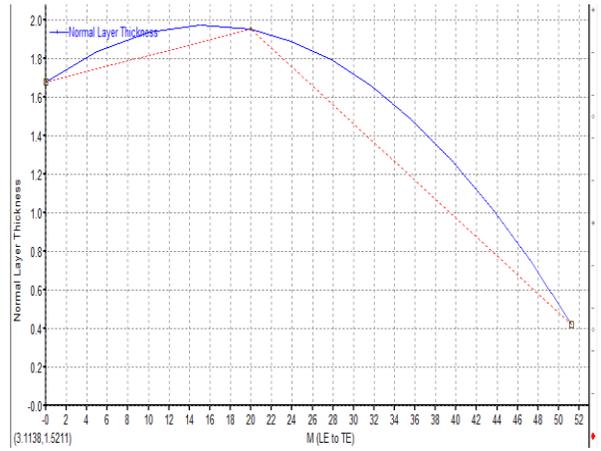
Fig 2.11: Normal Thickness trend for Stator 1 at hub
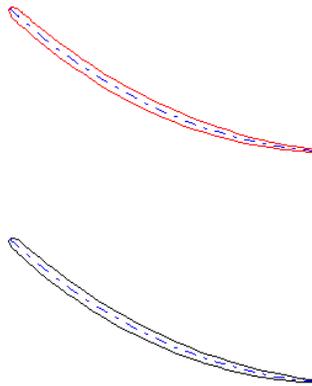
Fig 2.12: Blade Passage for Stator 1 at hub
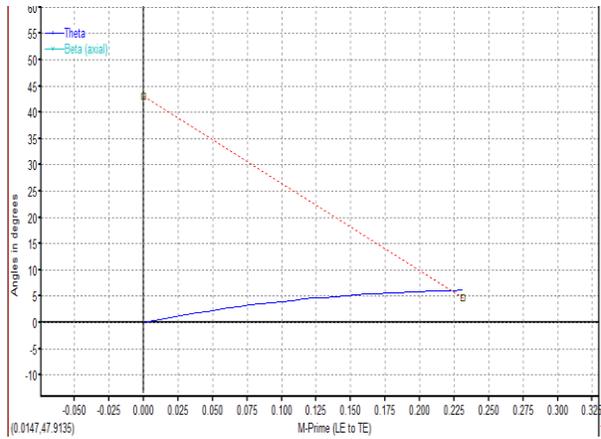
Fig 2.13: Beta over the airfoil for Stator 1 at hub
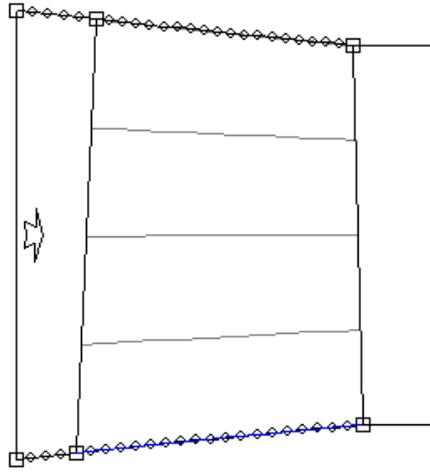
Fig 2.14:Meridional View for Rotor 2 at hub
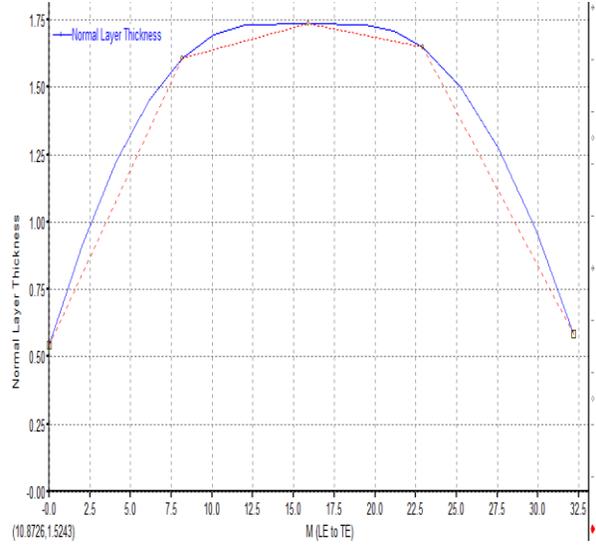
Fig 2.15: Normal Thickness trend for Rotor 2 at hub
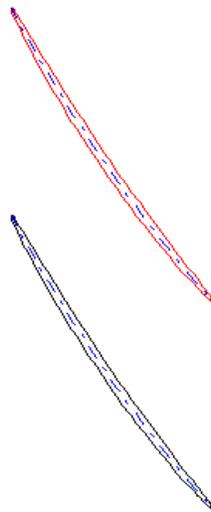
Fig 2.16: Blade Passage for Rotor 2 at hub
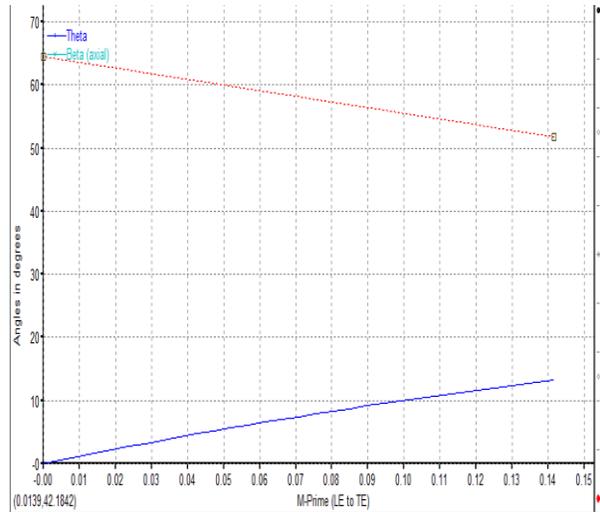
Fig 2.17: Beta over the airfoil for Rotor 2 at hub

2.2.2.2 Meshing

Meshing was done using ANSYS Turbogrid which allows simplified mesh generation specifically for turbomachinary. Automatic topology (ATM) is used for mesh creation which considers H grid, C grid, O grid and the combinations of those to make a mesh. The table below shows the node and element count for all components.

Table 2.3: Mesh Nodes and Elements

Component	Total Nodes	Total Elements
Rotor 1	249845	231268
Stator 1	112503	102772
Rotor 2	309820	287234
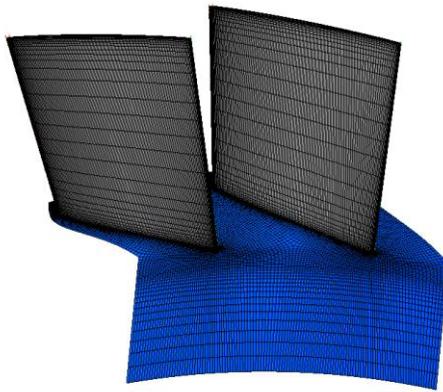
Figure 2.18: Rotor 1 Mesh
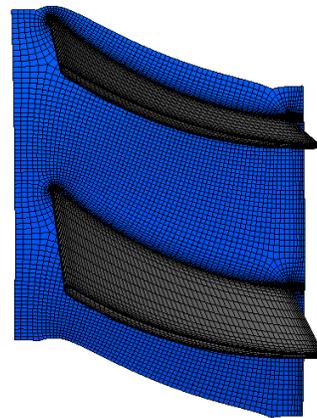
Fig 2.19: Stator 1 Mesh

Fig 2.20: Rotor 2 Mesh
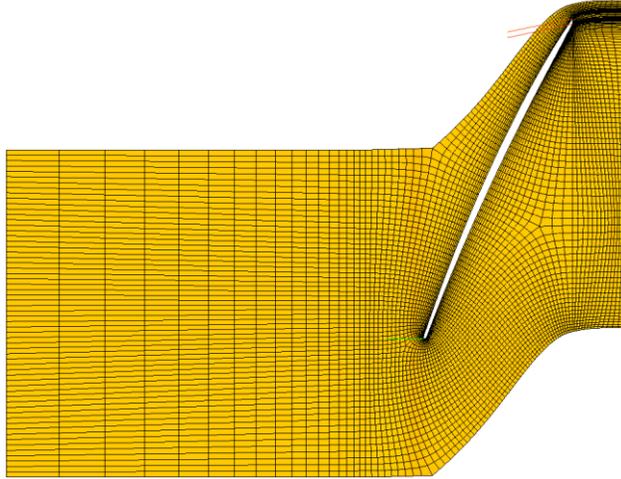
Fig 2.21: Rotor 1 grid
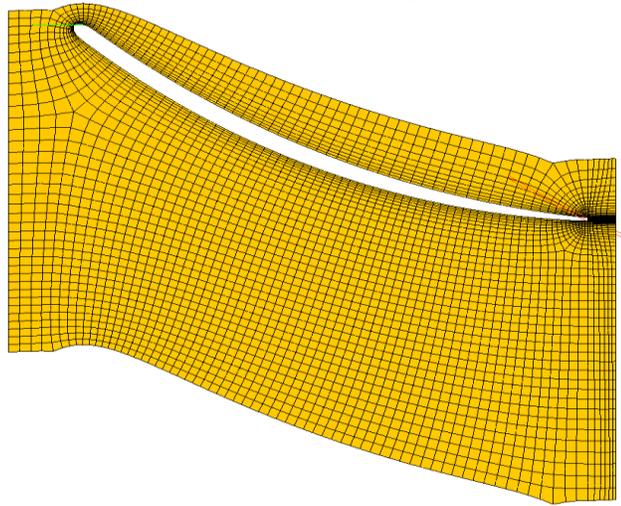
Fig 2.22: Stator 1 Grid
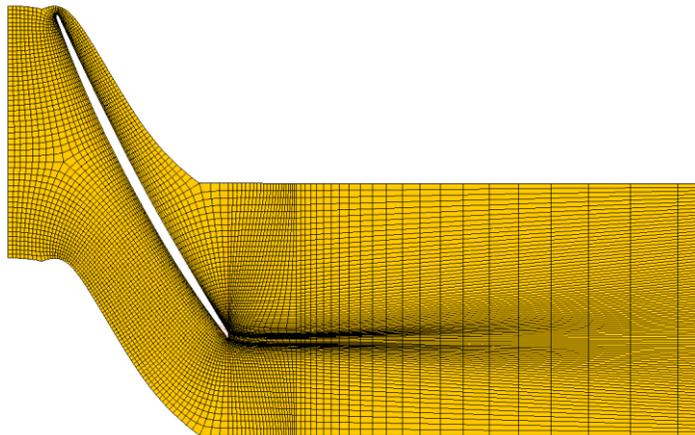
Fig 2.23: Rotor 2 Grid

2.2.2.3 Physical Setup in CFX Pre

After the mesh generation using turbogrid, CFX-Pre was used to setup the compressor for simulation. The figure below shows the compressor setup followed by the table of parameters used for the pre simulation setup. The conditions for the setup are directly taken from mean line analysis. The boundary condition used for the inlet is total pressure and temperature with static pressure as boundary condition for the outlet. K-epsilon is used for turbulence modelling with total energy as the energy model.

It can be noted here that the initial run used Shear State Transport turbulence model. However, it was found that the results were inconsistent with mean line analysis and it took several iterations to converge the solution. Also, thermodynamic properties were monitored during the convergence, and it was seen that temperature and pressure plots were not stable even after the residuals converged. It was then concluded that SST turbulence model may not be suitable for supersonic turbomachinary components and for that reason the turbulence model was switched to k-epsilon, which matched meanline analysis results and converged with great accuracy and speed.
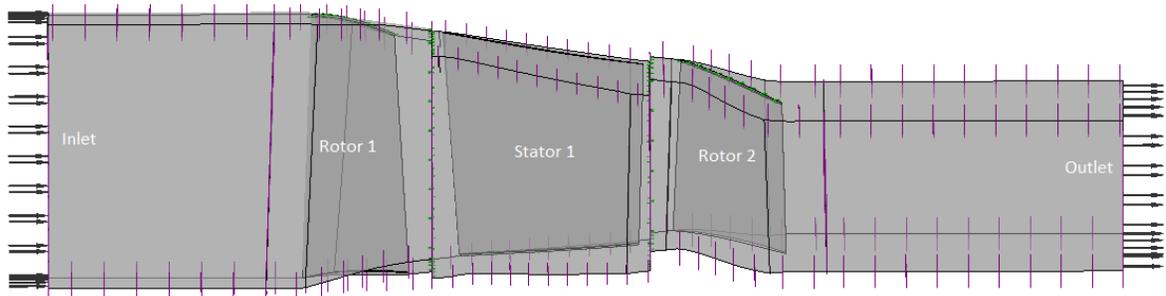
Fig 2.24: CFX-Pre compressor setup

Table 2.4: ANSYS Pre-Setup

Pre-processing Specification	
Analysis type	Steady state
Interference	Stage
Turbulence model	K-e
Wall function	Automatic
Advection scheme	High resolution
Timescale control	Auto timescale
Convergence criteria: Residual type Residual target	RMS 1E-4
Wall boundaries: Mass and momentum Wall roughness Heat transfer	No slip wall Smooth Adiabatic

3. Simulations

3.1 Introduction

In this section the final results of the simulations are discussed. As mentioned in the preceding chapters, the simulation was divided into three sections for analysis;

1. Design Point

2. Stall

3. Stall correction

Various key aerodynamics and thermodynamics parameters are taken into account to compare and contrast the results between the simulations.

3.2 Design Point

For Design point simulation, inlet and outlet boundary conditions are mentioned in Table 3.1 below.

Table 3.1: Boundary condition for Design point

Inlet (R1 in):	
Total pressure	339 kPa
Total temperature	488 K
Turbulence intensity	Medium (5%)
Outlet (R2 out):	
Static pressure	700 kPa

3.2.2 Numerical Vs CFD

Numerical (mean line) results were compared to CFD results in this section. The error between both was calculated to validate CFD results which was important not only for accurate results but to simulate conditions at Off-design. Key parameters were taken into account and are depicted in the table below at mean radius. Refer to Appendix for detailed numerical results.

Table 3.2: Design Point Numerical in comparison with CFD

Parameters	Numerical	CFD	Error %
Total Pressure	2.50	2.46	1.35
Inlet Beta	69.70°	69.74°	0.06
Inlet Alpha	0°	0°	0
Outlet Beta	-58.59°	-56.28°	3.94
Outlet Alpha	-36.35°	-34.34°	5.52
Mach (rel) Inlet	1.15	1.15	0
Mach (rel) Outlet	0.76	0.79	3.79

| Mach (abs) Inlet | 0.39 | 0.39 | 0 |
| Mach (abs) Outlet | 0.52 | 0.47 | 9.97 |

After analyzing and comparing the data between CFD and numerical results at design point it was concluded that CFD can be used for Off-design analysis.

3.2.3 Results

Mach Contour is of utmost importance for analyzing aerodynamic behavior of the compressor in this case, it helps to analyze shock placement and most importantly, study the regions of separation over the airfoil.

Shockwave can be seen at the entrance of the passage at Rotor 1 in the first stage. However, there are two shockwaves in Rotor 2. One shock is at the entrance and other shock is an ingested shockwave. It must be noted that the counter-rotating Rotor 2 sees a higher relative velocity due the opposing velocity triangles (See Fig) which results in a higher relative Mach value for Rotor 2.
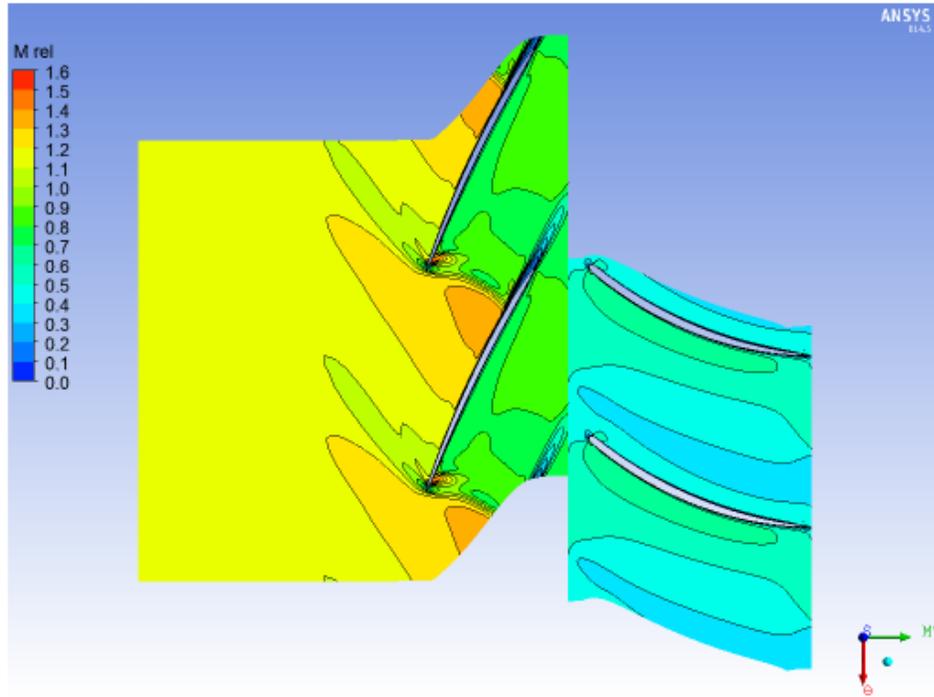
Fig 3.1: Relative Mach Contours for Rotor 1 at Deign Point

Fig 3.2: Relative Mach Contours for Rotor 2 at Deign Point

Fig 3.3: Relative Velocity Contours and Vectors for Rotor 1 at Design Point
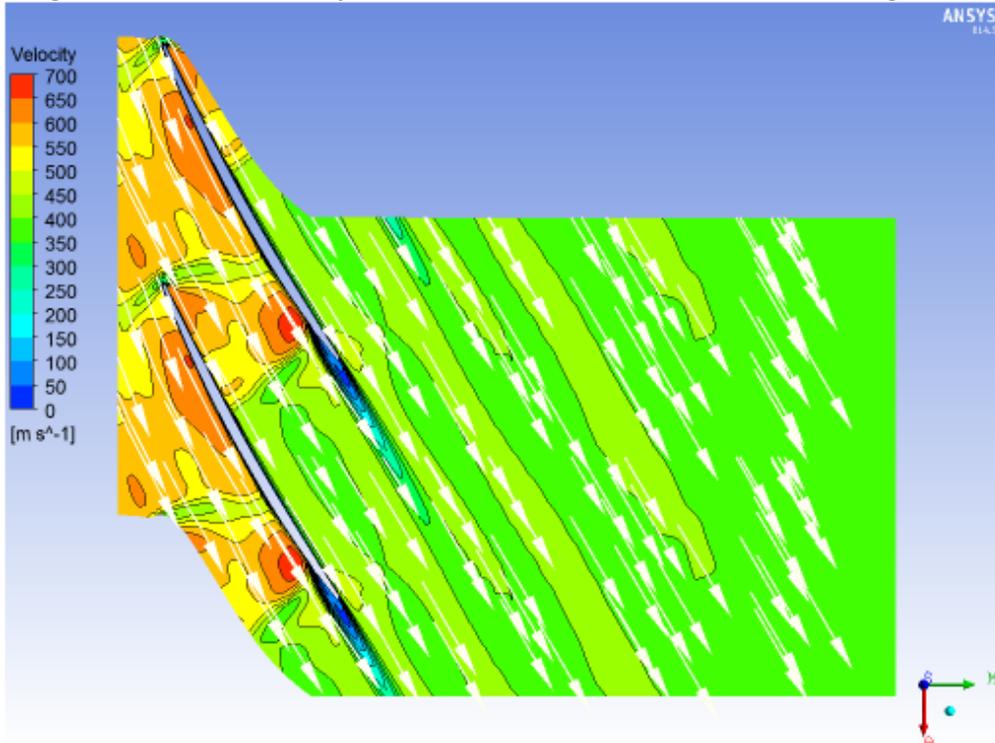
Fig 3.4: Relative Velocity Contours and Vectors for Rotor 2 at Design Point

The below figures show absolute (Alpha) and relative (Beta) angles along the span for various airfoils.
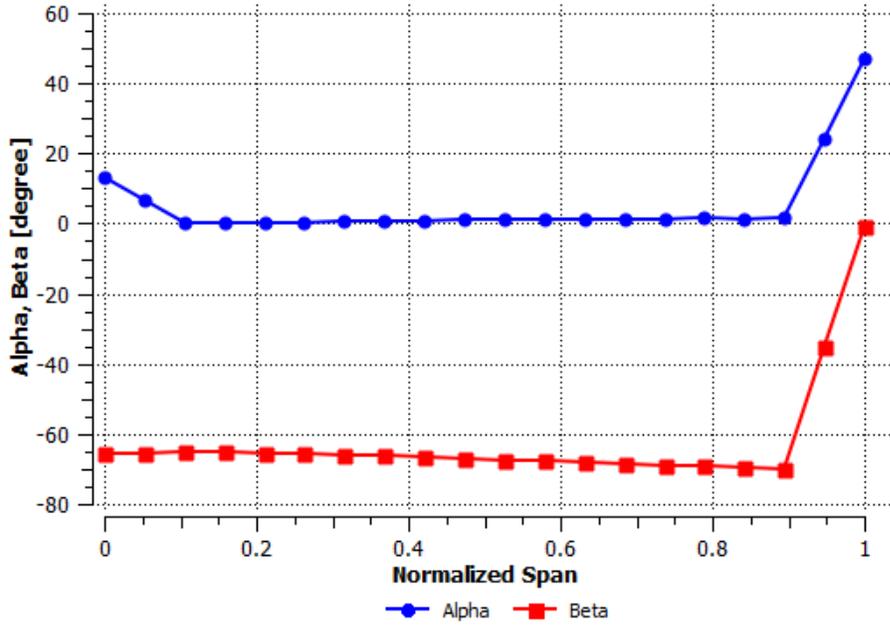
Fig 3.5: Rotor 1 inlet alpha and beta along the span
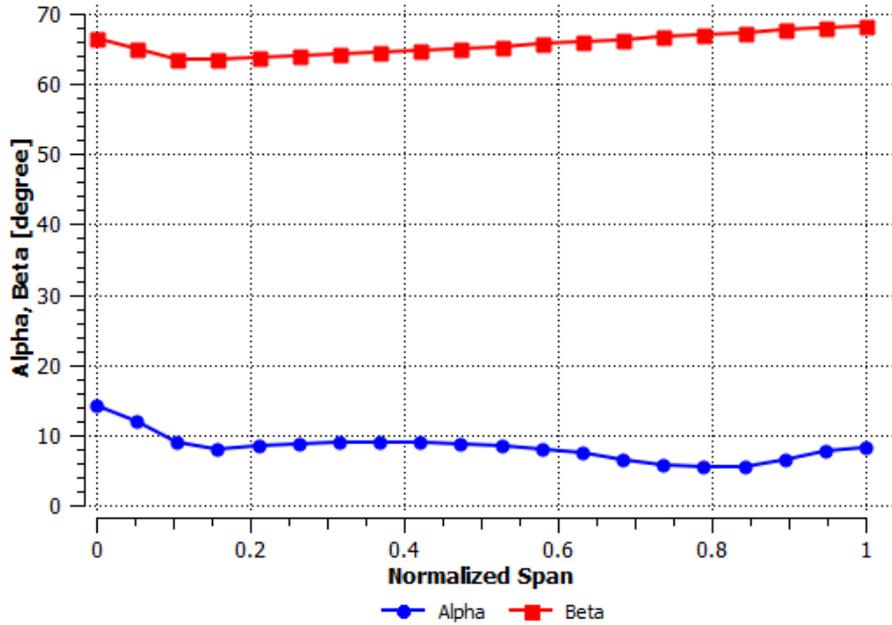
Fig 3.6: Rotor 2 inlet alpha and beta along the span

The following figures are Mach number blade loading charts along the stream wise direction. The plots give Mach number over the pressure and suction surface of the airfoil. The steep decline in Mach number suggests a shockwave.
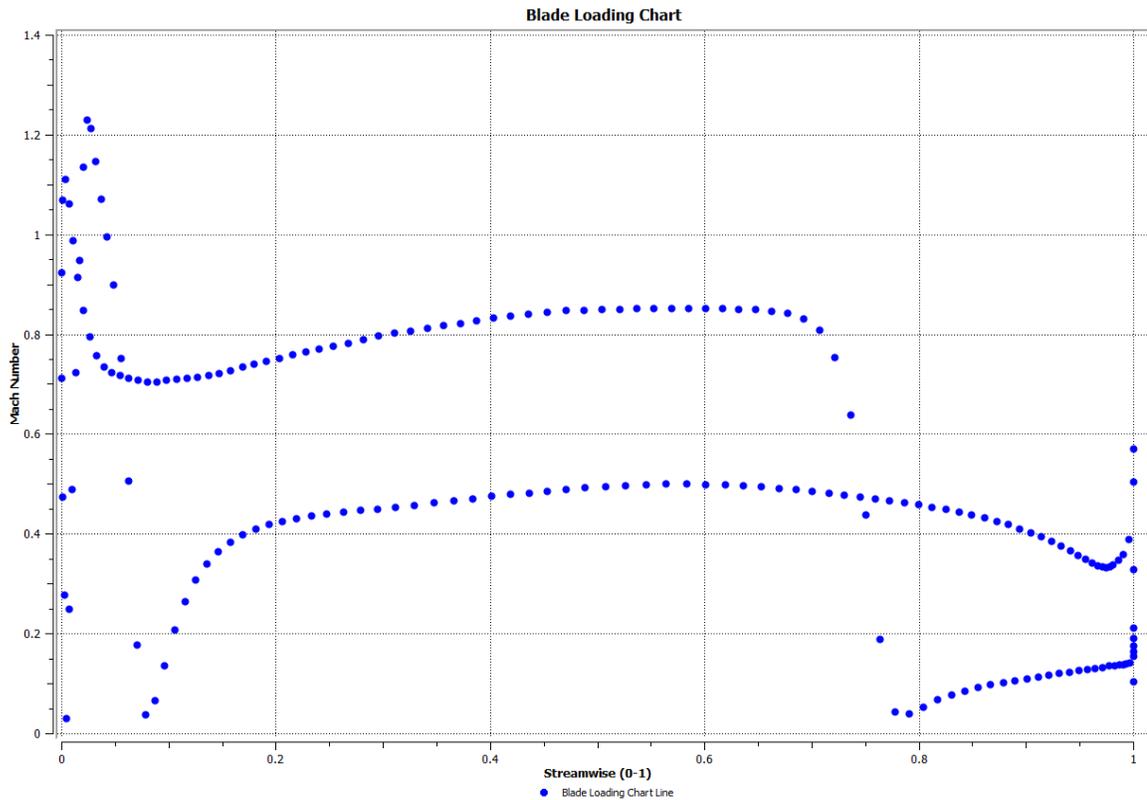
Fig 3.7: Mach number blade loading at 50% span for Rotor 1

From the figure above it can be seen that there is shockwave at 80% of the stream wise location. Comparing the chart above with Mach countours from figure XX it can be noted that a shock is present at the mouth of the passage.
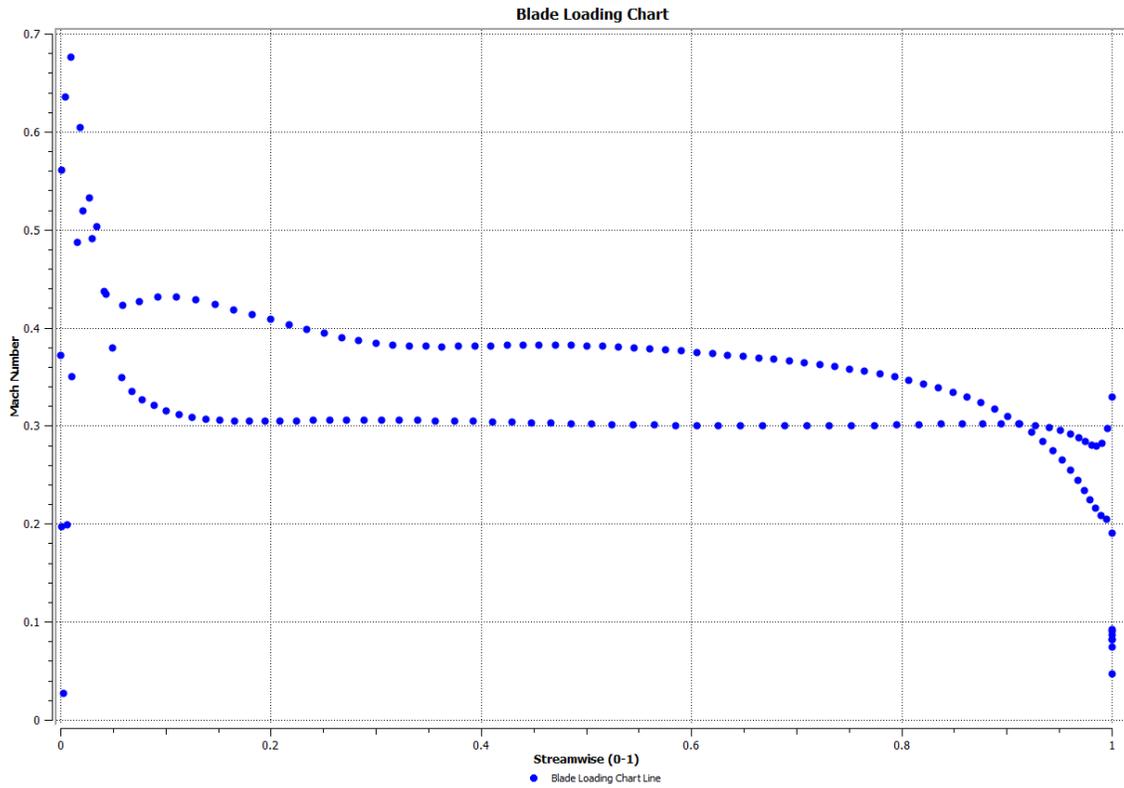
Fig 3.8: Mach number blade loading at 50% span for Stator 1

The figure above shows the Mach number profile over the stator 1 at 50% of the span. It

can be seen that the Mach number everywhere is < 1 suggesting that the flow is subsonic.

The figure below shows Mach number blade profile of Rotor 2. The flow is highly

supersonic due to the nature of the counter-rotating design which increases the relative

Mach number at the inlet of Rotor 2.
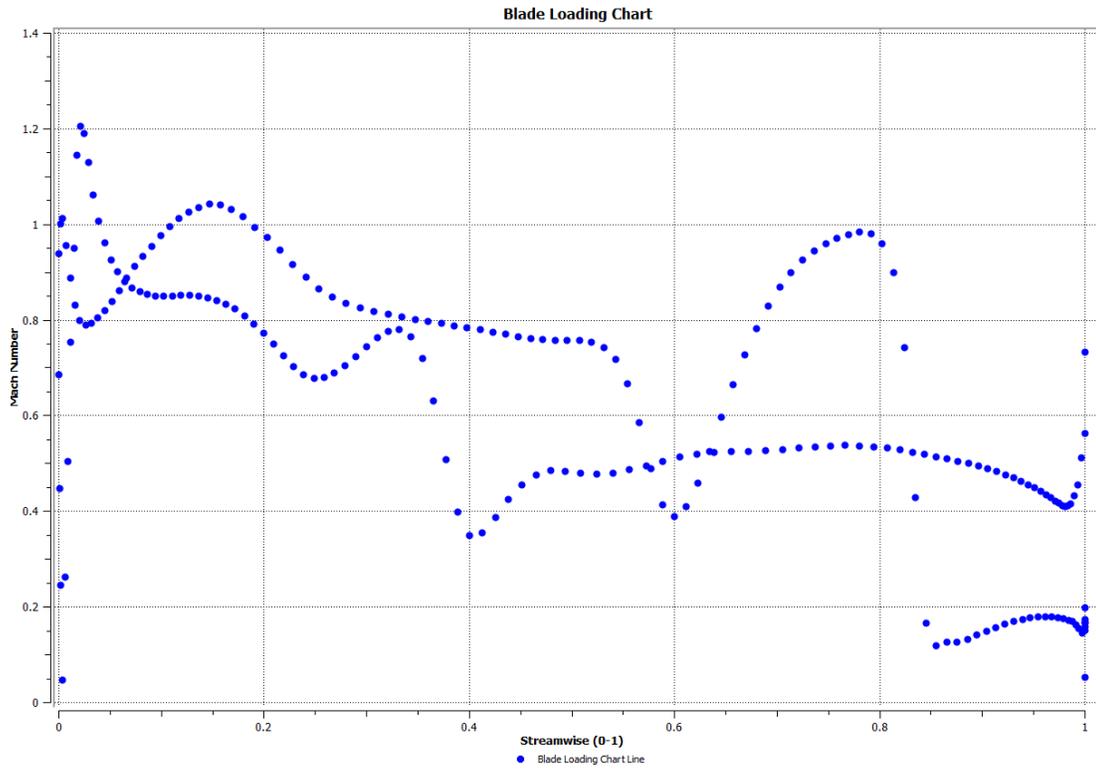
Fig 3.9: Mach number blade loading at 50% span for Rotor 2

Following are the detailed summary of the results from CFX Post analysis at design point.

Table 3.3: Performance Summary at Design Point

Inlet Mass Flow Rate	59.5056	[kg s^-1]
Inlet Volume Flow Rate	18.9135	[m^3 s^-1]
Total Pressure Ratio	2.1292	
Total Temperature Ratio	1.3026	
Total-to-Total Isentropic Efficiency %	80.1990	
Total-to-Total Polytropic Efficiency %	82.1710	

It can be noted from the table above that the pressure ratio is 2.129, however after doing further analysis it was found that pressure ratio calculated in the table above by CFX is not calculated from domain inlet and outlet but from LE to TE. Since the mean line

analysis calculations used the inlet and outlet domain it is necessary to recalculate CFX results in the same way.

The table below shows detailed thermodynamic and aerodynamic properties for Rotor 1. It can be noted from the flow angles that the change is beta from inlet to outlet is only 6.58°.

Table 3.4: Thermodynamic and Aerodynamic Properties for Rotor 1

Quantity	Inlet	LE Cut	TE Cut	Outlet	TE/LE	TE-LE	Units
Density	2.9093	2.8227	3.6473	3.6506	1.2921	N/A	[kg m^-3]
Pstatic	293710.0000	283810.0000	460135.0000	459302.0000	1.6213	176325.0000	[Pa]
Pt	339477.0000	341586.0000	578905.0000	559267.0000	1.6948	237319.0000	[Pa]
Pt (rot)	339308.0000	325693.0000	302121.0000	305735.0000	0.9276	-23572.0000	[Pa]
T	472.9470	470.0080	532.8800	532.6390	1.1338	62.8721	[K]
Tt	488.0040	489.1070	559.7020	558.6270	1.1443	70.5955	[K]
Tt (rot)	487.9540	487.9580	487.9440	487.9540	1.0000	-0.0145	[K]
H	175566.0000	172614.0000	235763.0000	235521.0000	1.3658	63148.8000	[J kg^-1]
Ht	190689.0000	191797.0000	262703.0000	261623.0000	1.3697	70906.1000	[J kg^-1]
Ht adiabatic	190689.0000	189535.0000	252145.0000	250855.0000	1.3303	62609.9000	[J kg^-1]
Ht polytropic	190689.0000	189527.0000	252787.0000	251421.0000	1.3338	63260.1000	[J kg^-1]
Rothalpy	190639.0000	190643.0000	190629.0000	190639.0000	0.9999	-14.5625	[J kg^-1]
Entropy	72.7763	77.4271	91.3926	92.1649	1.1804	13.9655	[J kg^-1 K^-1]
Mach (abs)	0.3988	0.4467	0.5139	0.4886	1.1503	0.0671	
Mach (rel)	1.1594	1.1527	0.7485	0.7753	0.6494	-0.4041	
U	474.6230	474.6330	474.8120	474.0930	1.0004	0.1790	[m s^-1]
Cm	173.8680	186.4500	157.5670	160.8970	0.8451	-28.8834	[m s^-1]
Cu	0.1169	9.8835	168.5280	154.7660	17.0515	158.6450	[m s^-1]
C	173.8910	194.7030	239.1200	226.5010	1.2281	44.4172	[m s^-1]
Wu	-474.5060	-464.7500	-306.2840	-319.3270	0.6590	158.4660	[m s^-1]
W	505.5740	501.3610	346.6770	359.3480	0.6915	-154.6840	[m s^-1]
Distortion Parameter	1.0003	1.0474	1.2015	1.0186	1.1471	N/A	
Flow Angle: Alpha	0.0453	4.3275	45.1457	44.1500	N/A	40.8181	[degree]
Flow Angle: Beta	-69.7499	-63.2882	-60.5593	-63.1445	N/A	2.7288	[degree]

The table below shows detailed thermodynamic and aerodynamic properties for Stator 1.

It can be noted from the flow angle that the difference between the inlet and outlet is

33.44°. High amount of swirl was taken out to reduce the relative Mach number for Rotor

2, making the chord of the stator long.

Table 3.5: Thermodynamic and Aerodynamic Properties for Stator 1

Quantity	Inlet	LE Cut	TE Cut	Outlet	TE/LE	TE-LE	Units
Density	3.6495	3.6067	3.6594	3.6523	1.0146	N/A	[kg m^-3]
Pstatic	459318.0000	451679.0000	462364.0000	460877.0000	1.0237	10685.0000	[Pa]
Ptotal	559085.0000	553677.0000	551042.0000	551708.0000	0.9952	-2635.0000	[Pa]
Tstatic	532.7220	530.2330	534.9440	534.1420	1.0089	4.7104	[K]
Ttotal	558.7250	558.6810	558.8050	558.7540	1.0002	0.1244	[K]
Hstatic	235604.0000	233104.0000	237836.0000	237030.0000	1.0203	4731.2000	[J kg^-1]
Htotal	261721.0000	261677.0000	261802.0000	261751.0000	1.0005	124.9220	[J kg^-1]
Entropy	92.3371	92.9587	94.7706	94.8067	1.0195	1.8119	[J kg^-1 K^-1]
Mach	0.4880	0.4875	0.4550	0.4609	0.9334	-0.0324	
Cm	160.7700	168.5780	207.2820	208.4610	1.2296	38.7034	[m s^-1]
Cu	154.7520	146.3350	30.8002	29.8529	0.2105	-115.5340	[m s^-1]
C	226.2310	225.1240	210.9980	213.5520	0.9373	-14.1257	[m s^-1]
Distortion Parameter	1.0191	1.1317	1.0751	1.0860	0.9500	N/A	
Flow Angle	44.1967	41.3767	7.9323	7.3794	N/A	-33.4444	[degree]

The table below shows detailed thermodynamic and aerodynamic properties for Rotor 2. It must be noted from the results that the absolute flow angle switches sign from positive to negative, suggesting counter-rotating behavior of the rotor. It can also be seen that all the angles are within the aerodynamic limits. The total pressure at the exit of the rotor 2 is 837213 Pa, while the inlet total pressure at the rotor 1 is 339477 Pa which results in total pressure ratio of 2.46.

Table 3.6: Thermodynamic and Aerodynamic Properties for Rotor 1

Quantity	Inlet	LE Cut	TE Cut	Outlet	TE/LE	TE-LE	Units
Density	3.6547	3.5618	4.5248	4.5909	1.2704	N/A	[kg m^-3]
Pstatic	460822.0000	445570.0000	686663.0000	700759.0000	1.5411	241093.0000	[Pa]
Pt	551847.0000	554943.0000	866192.0000	837214.0000	1.5609	311249.0000	[Pa]
Pt (rot)	612493.0000	610266.0000	546679.0000	554125.0000	0.8958	-63587.3000	[Pa]
T	533.9320	530.7530	602.6370	607.5140	1.1354	71.8837	[K]
Tt	558.5730	559.5440	636.0920	635.6940	1.1368	76.5472	[K]
Tt (rot)	573.6280	573.9870	574.0790	574.0630	1.0002	0.0928	[K]
H	236819.0000	233627.0000	305827.0000	310725.0000	1.3090	72200.0000	[J kg^-1]
Ht	261568.0000	262545.0000	339429.0000	339029.0000	1.2928	76884.1000	[J kg^-1]
Ht adiabatic	249574.0000	248170.0000	312154.0000	309122.0000	1.2578	63983.7000	[J kg^-1]
Ht polytropic	250193.0000	248913.0000	314911.0000	312098.0000	1.2651	65997.8000	[J kg^-1]
Rothalpy	276690.0000	277050.0000	277143.0000	277127.0000	1.0003	93.1875	[J kg^-1]
Entropy	94.4416	98.7628	116.2800	120.8680	1.1774	17.5172	[J kg^-1 K^-1]
Mach (abs)	0.4618	0.5150	0.5389	0.4781	1.0465	0.0239	
Mach (rel)	1.1741	1.2021	0.7750	0.7944	0.6447	-0.4271	
U	472.9650	472.6570	472.6030	472.5760	0.9999	-0.0534	[m s^-1]
Cm	208.6000	227.2480	202.4820	194.8790	0.8910	-24.7661	[m s^-1]
Cu	28.9944	31.2352	-152.1130	-132.2040	-4.8699	-183.3480	[m s^-1]
C	213.9250	237.5360	266.4840	236.3880	1.1219	28.9483	[m s^-1]
Wu	501.9590	503.8920	320.4910	340.3720	0.6360	-183.4020	[m s^-1]
W	544.5360	553.6480	381.8730	392.8910	0.6897	-171.7750	[m s^-1]
Distortion Parameter	1.0823	1.0374	1.1354	1.0086	1.0945	N/A	
Flow Angle: Alpha	6.9258	8.0610	-30.5601	-34.3421	N/A	-38.6211	[degree]
Flow Angle: Beta	67.5269	65.6525	59.0274	60.1635	N/A	-6.6252	[degree]

3.3 Stall

Stall conditions were induced within the compressor by incrementally increasing static

back pressure at the outlet for Rotor 2. The simulation did not converge due to unstable

residuals which occurred from backflow and recirculation at stall conditions. Therefore, the iterations were stopped at 50% backflow conditions.

For Stall simulation, inlet and outlet boundary conditions are mentioned in Table below.

Table 3.7: Boundary condition for Design point

Inlet (R1 in):	
Total pressure	339 kPa
Total temperature	488 K
Turbulence intensity	Medium (5%)
Outlet (R2 out):	
Static pressure	860 kPa

3.3.1 Results

Mach Contours and velocity counters are analyzed to study stall. It can be seen from the figures below that Stator 1 and Rotor 2 have completely stalled with recirculation. Further detailed summary can be seen in Table 3.9.
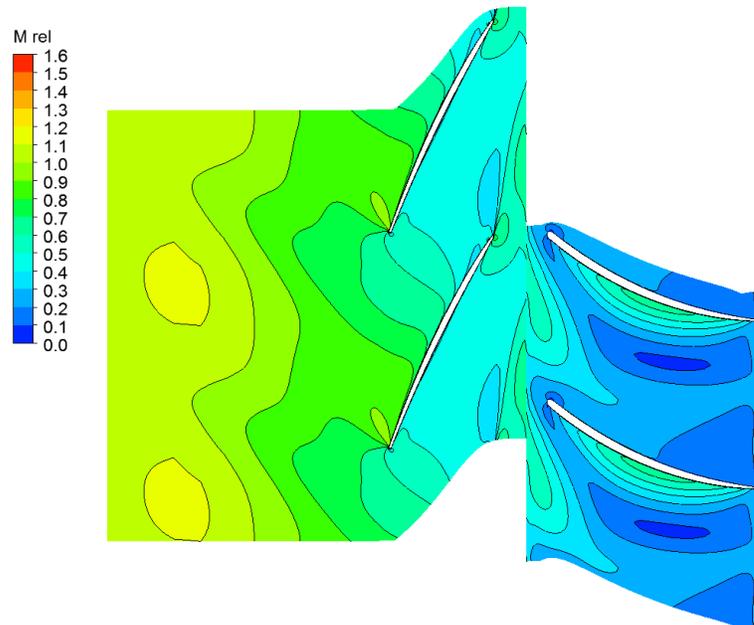
Fig 3.10: Relative Mrel Contour for Rotor 1 at Stall
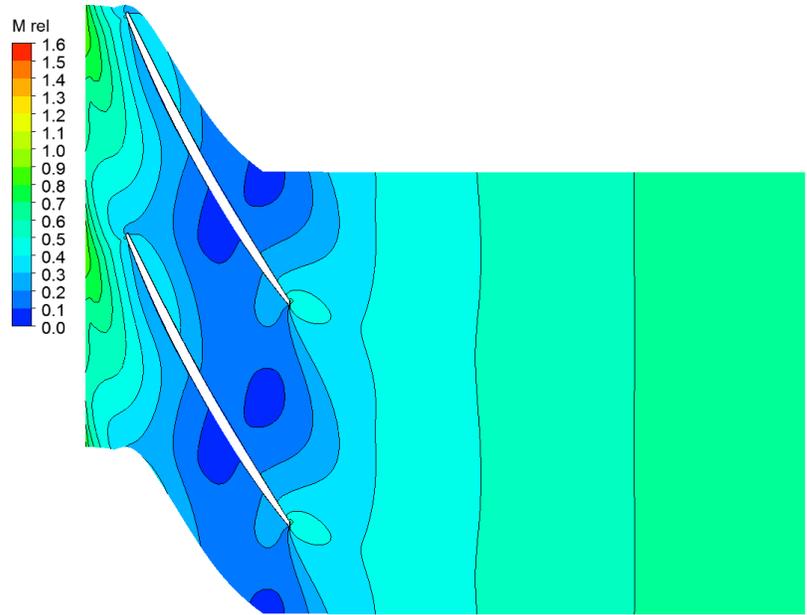
Fig 3.11: Relative Mrel Contour for Rotor 2 at Stall
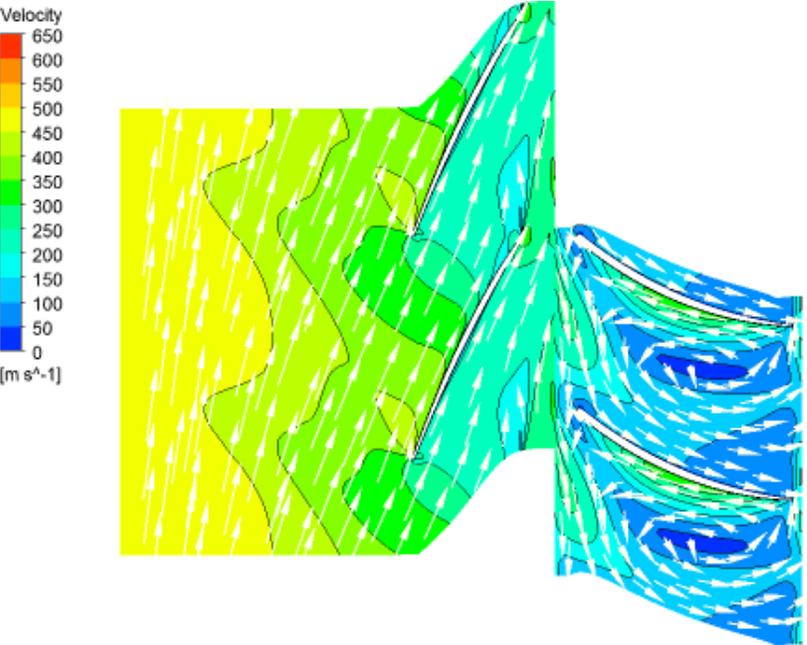
Fig 3.12: Relative Velocity Contour for Rotor 1 at Stall
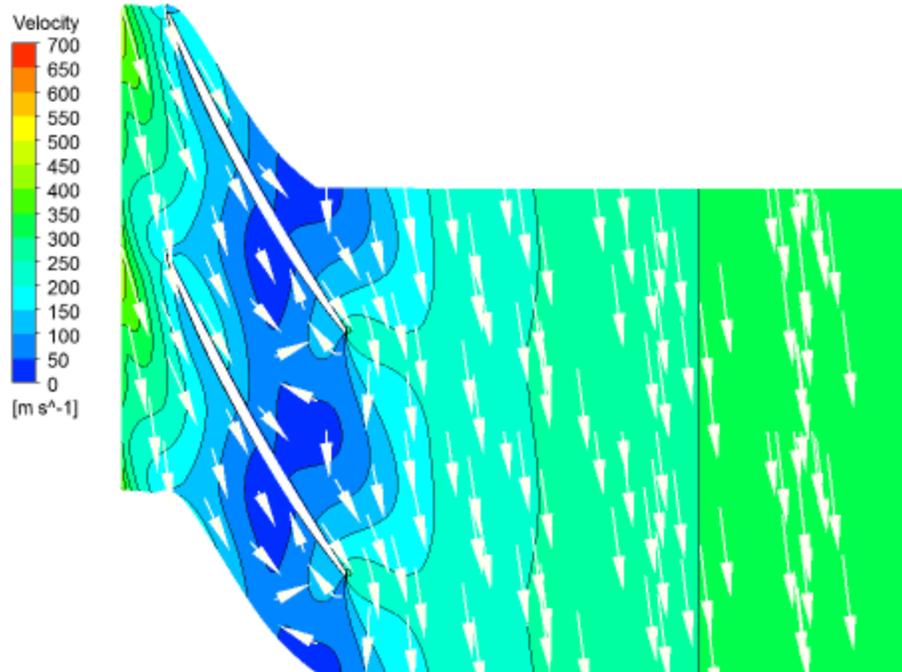
Fig 3.13: Relative Velocity Contour for Rotor 2 at Stall

Table 3.8 below shows the performance of the stalled compressor. It can be noted that mass flow at stalled condition is merely 15 Kg/s, this is due to high back pressure which results in lowering the mass flow. However, the pressure ratio is higher than the design point values due to an overall increase in pressure.

Table 3.8: Performance characteristics at stalled condition

Inlet Mass Flow Rate	15.0079	[kg s^-1]
Inlet Volume Flow Rate	4.7137	[m^3 s^-1]
Total Pressure Ratio	2.2663	
Total Temperature Ratio	1.3259	
Total-to-Total Isentropic Efficiency %	82.1680	
Total-to-Total Polytropic Efficiency %	84.1089	

The table below shows detailed thermodynamic and aerodynamic properties for Rotor 1 at stalled condition. It must be noted that inlet angle is now 40° even though the specified angle for the simulation is pure axial flow. This could be due to multiple reasons like unconverged solution, unstable and oscillating residuals, etc.

Table 3.9: Thermodynamic and Aerodynamic Properties for Rotor 1

Quantity	Inlet	LE Cut	TE Cut	Outlet	TE/LE	TE-LE	Units
Density	3.1555	2.6077	4.0796	4.1379	1.5645	N/A	[kg m^-3]
Pstatic	340857.0000	304994.0000	589190.0000	592097.0000	1.9318	284197.0000	[Pa]
Pt	346415.0000	692526.0000	843543.0000	700914.0000	1.2181	151017.0000	[Pa]
Pt (rot)	340933.0000	194904.0000	283529.0000	341293.0000	1.4547	88625.0000	[Pa]
T	485.1810	429.3100	566.4230	586.2960	1.3194	137.1130	[K]
Tt	487.9120	267.4070	611.2930	624.8450	2.2860	343.8860	[K]
Tt (rot)	487.9170	489.2140	487.2450	500.2480	0.9960	-1.9686	[K]
H	187854.0000	131737.0000	269453.0000	289414.0000	2.0454	137716.0000	[J kg^-1]
Ht	190597.0000	-30878.7000	314521.0000	328132.0000	-10.1857	345399.0000	[J kg^-1]
Ht adiabatic	190597.0000	7899.4300	304458.0000	297160.0000	38.5418	296559.0000	[J kg^-1]
Ht polytropic	190597.0000	-8841.2400	306018.0000	300120.0000	-34.6125	314859.0000	[J kg^-1]
Rothalpy	190602.0000	191905.0000	189927.0000	202987.0000	0.9897	-1977.2500	[J kg^-1]
Entropy	72.5549	63.3253	87.3643	121.3360	1.3796	24.0390	[J kg^-1 K^-1]
Mach (abs)	0.1246	0.7795	0.6613	0.4446	0.8483	-0.1183	
Mach (rel)	1.0728	0.6904	0.4062	0.5835	0.5884	-0.2842	
U	474.6230	474.6330	474.8120	474.0930	1.0004	0.1790	[m s^-1]
Cm	53.5865	135.9430	86.5775	70.1384	0.6369	-49.3655	[m s^-1]
Cu	3.2550	286.4560	308.1210	201.5790	1.0756	21.6648	[m s^-1]
C	55.1313	369.1190	322.3980	215.4700	0.8734	-46.7210	[m s^-1]
Wu	-471.3680	-188.1770	-166.6910	-272.5140	0.8858	21.4859	[m s^-1]
W	475.2140	312.0080	197.2840	283.7160	0.6323	-114.7240	[m s^-1]
Distortion Parameter	1.5022	2.2986	1.1756	1.1650	0.5114	N/A	
Flow Angle: Alpha	40.2149	55.3878	84.1022	84.6001	N/A	28.7145	[degree]
Flow Angle: Beta	19.2295	-1.0675	33.3217	26.2289	N/A	34.3892	[degree]

The table below shows detailed thermodynamic and aerodynamic properties for Stator 1. The flow angle is very high and above the criteria which is due to recirculation at the suction surface of the blade.

Table 3.10: Summary of Stator 1 at stall

Quantity	Inlet	LE Cut	TE Cut	Outlet	TE/LE	TE-LE	Units
Density	4.1274	4.0250	4.0543	3.9261	1.0073	N/A	[kg m^-3]
Pstatic	592559.0000	596255.0000	611395.0000	604428.0000	1.0254	15140.3000	[Pa]
Ptotal	691340.0000	675112.0000	731859.0000	860410.0000	1.0841	56747.6000	[Pa]
Tstatic	584.1820	590.2340	545.4460	546.0540	0.9241	-44.7881	[K]
Ttotal	622.7510	623.2710	515.6170	505.5860	0.8273	-107.6540	[K]
Hstatic	287291.0000	293369.0000	248384.0000	248995.0000	0.8467	-44985.2000	[J kg^-1]
Htotal	326030.0000	326552.0000	218423.0000	208349.0000	0.6689	-108128.0000	[J kg^-1]
Entropy	117.9810	139.0340	62.7222	72.4810	0.4511	-76.3115	[J kg^-1 K^-1]
Mach	0.4205	0.3636	0.3696	0.5471	1.0165	0.0060	
Cm	69.6553	57.6357	82.9734	97.5145	1.4396	25.3377	[m s^-1]
Cu	189.8250	164.5960	-125.3150	-217.5300	-0.7613	-289.9110	[m s^-1]
C	204.0920	178.1340	186.8120	281.1520	1.0487	8.6787	[m s^-1]
Distortion Parameter	1.2367	1.5023	3.1116	2.3226	2.0712	N/A	
Flow Angle	85.1736	88.1750	53.5462	55.0176	N/A	-34.6288	[degree]

The table below shows detailed thermodynamic and aerodynamic properties for Rotor 2. The inlet beta is 102.4° which is extremely high and above the aerodynamic health criteria. It can also be noted that due to the recirculation of the flow, the outlet alpha angle has the same sign as the inlet alpha angle suggesting that the flow is not counter-rotating

Table 3.11: Thermodynamic and Aerodynamic Properties for Rotor 2

Quantity	Inlet	LE Cut	TE Cut	Outlet	TE/LE	TE-LE	Units
Density	3.9104	3.8462	4.6164	5.1885	1.2003	N/A	[kg m^-3]
Pstatic	604595.0000	599733.0000	777296.0000	854372.0000	1.2961	177563.0000	[Pa]
Pt	867281.0000	1078200.0000	1058050.0000	913403.0000	0.9813	-20152.8000	[Pa]
Pt (rot)	446347.0000	411741.0000	452001.0000	607019.0000	1.0978	40260.3000	[Pa]
T	547.0180	540.3620	623.5300	637.1260	1.1539	83.1676	[K]
Tt	504.5370	467.5250	654.9780	646.9190	1.4009	187.4530	[K]
Tt (rot)	594.2830	594.2300	599.0990	595.4020	1.0082	4.8693	[K]
H	249963.0000	243278.0000	326811.0000	340467.0000	1.3434	83533.5000	[J kg^-1]
Ht	207295.0000	170120.0000	358398.0000	350303.0000	2.1067	188278.0000	[J kg^-1]
Ht adiabatic	217995.0000	175355.0000	321614.0000	321740.0000	1.8341	146259.0000	[J kg^-1]
Ht polytropic	212700.0000	167139.0000	325584.0000	324849.0000	1.9480	158445.0000	[J kg^-1]
Rothalpy	297436.0000	297383.0000	302274.0000	298560.0000	1.0165	4890.6600	[J kg^-1]
Entropy	74.2511	95.7280	130.3860	117.7020	1.3620	34.6585	[J kg^-1 K^-1]
Mach (abs)	0.5512	0.7443	0.6270	0.2921	0.8423	-0.1173	
Mach (rel)	0.6054	0.5527	0.4095	0.6734	0.7409	-0.1432	
U	472.9650	472.6570	472.6030	472.5760	0.9999	-0.0534	[m s^-1]
Cm	97.7167	108.2020	101.9540	51.1835	0.9423	-6.2476	[m s^-1]
Cu	-222.1430	-310.0880	-292.0290	-135.3800	0.9418	18.0586	[m s^-1]
C	284.0220	380.1100	324.0830	148.3780	0.8526	-56.0271	[m s^-1]
Wu	250.8210	162.5690	180.5740	337.1960	1.1107	18.0051	[m s^-1]
W	297.2900	270.5380	209.8580	342.0230	0.7757	-60.6805	[m s^-1]
Distortion Parameter	2.3408	1.8892	1.1053	1.0351	0.5851	N/A	
Flow Angle: Alpha	55.3564	72.3515	73.8511	56.1766	N/A	1.4996	[degree]
Flow Angle: Beta	102.4770	123.5630	83.5486	84.5058	N/A	-40.0148	[degree]

The blade loading case is not studied at the stall condition since it would be irrelevant due to the stalled nature of the compressor.

3.4 Active Stall Control

As mentioned previously, the stall is corrected by changing the RPM of the second rotor and keeping all else the stall same (See Table). The RPM is changed from 18000 to 21000. The solution was completely converged and all the residual criteria were met.

3.4.1 Results

The following represents the performance of the compressor after stall control.

Table 3.12: Performance Characteristics at Stall Control

Inlet Mass Flow Rate	62.3991	[kg s^-1]
Inlet Volume Flow Rate	19.8338	[m^3 s^-1]
Total Pressure Ratio	2.5724	
Total Temperature Ratio	1.3823	
Total-to-Total Isentropic Efficiency %	81.5058	
Total-to-Total Polytropic Efficiency %	83.7728	

It can be noted from the table above that the pressure ratio is 2.57 which is a little higher than the design point pressure ratio due to the increased static back pressure condition and the higher RPM of rotor 2.

The table below shows the thermodynamic and aerodynamic properties of Rotor 1 after applying active stall control to the compressor system. It can be noted that all the properties lie within the criteria.

Table 3.13: Aerodynamic and thermodynamic properties for Rotor 1

Quantity	Inlet	LE Cut	TE Cut	Outlet	TE/LE	TE-LE	Units
Density	2.8813	2.7428	3.7327	3.7542	1.3609	N/A	[kg m^-3]
Pstatic	288396.0000	272774.0000	492284.0000	493365.0000	1.8047	219510.0000	[Pa]
Pt	339464.0000	345736.0000	663422.0000	622034.0000	1.9189	317686.0000	[Pa]
Pt (rot)	339235.0000	315099.0000	279741.0000	286297.0000	0.8878	-35357.9000	[Pa]
T	471.1230	467.0730	547.2940	547.4860	1.1718	80.2209	[K]
Tt	488.0040	489.2700	581.5490	579.7280	1.1886	92.2794	[K]
Tt (rot)	487.9360	487.9300	488.0150	487.9780	1.0002	0.0848	[K]
H	173735.0000	169666.0000	250240.0000	250433.0000	1.4749	80573.9000	[J kg^-1]
Ht	190689.0000	191961.0000	284646.0000	282817.0000	1.4828	92685.4000	[J kg^-1]
Ht adiabatic	190689.0000	188684.0000	267557.0000	265276.0000	1.4180	78873.4000	[J kg^-1]
Ht polytropic	190689.0000	188638.0000	268816.0000	266402.0000	1.4250	80178.1000	[J kg^-1]
Rothalpy	190621.0000	190615.0000	190700.0000	190663.0000	1.0005	85.1719	[J kg^-1]
Entropy	72.7851	79.6718	101.8410	103.3440	1.2783	22.1692	[J kg^-1 K^-1]
Mach (abs)	0.4231	0.5005	0.5844	0.5345	1.1675	0.0839	
Mach (rel)	1.2836	1.2587	0.7740	0.8145	0.6149	-0.4847	
U	527.3590	527.3700	527.5690	526.7700	1.0004	0.1989	[m s^-1]
Cm	184.0930	203.3560	163.6730	164.1930	0.8049	-39.6824	[m s^-1]
Cu	0.1436	20.9526	208.4560	183.6250	9.9489	187.5030	[m s^-1]
C	184.1210	218.8480	276.8060	251.6460	1.2648	57.9582	[m s^-1]
Wu	-527.2160	-506.4180	-319.1130	-343.1450	0.6301	187.3040	[m s^-1]
W	558.6590	546.4210	363.8250	383.2560	0.6658	-182.5960	[m s^-1]
Distortion Parameter	1.0003	1.1249	1.2854	1.0262	1.1427	N/A	
Flow Angle: Alpha	0.0518	5.9572	49.7404	48.5131	N/A	43.7832	[degree]
Flow Angle: Beta	-70.6273	-60.8767	-56.4937	-64.4103	N/A	4.3830	[degree]

.

The following table depicts the data for Stator 1 after stall mitigation. The inlet flow

angle is 48.55 while the outlet flow angle is 7.25. It must be noted here that due to the

focus on stall mitigation using RPM change, a variable stator vane is not used.

Table 3.14: Summary of Stator 1 after stall recovery

Quantity	Inlet	LE Cut	TE Cut	Outlet	TE/LE	TE-LE	Units
Density	3.7527	3.6910	3.8323	3.8287	1.0383	N/A	[kg m^-3]
Pstatic	493438.0000	482321.0000	511917.0000	510975.0000	1.0614	29596.0000	[Pa]
Ptotal	621482.0000	610239.0000	606946.0000	607605.0000	0.9946	-3293.8800	[Pa]
Tstatic	547.6200	543.5490	555.1240	554.5670	1.0213	11.5748	[K]
Ttotal	579.8920	579.8620	579.9550	579.8400	1.0002	0.0925	[K]
Hstatic	250568.0000	246479.0000	258105.0000	257545.0000	1.0472	11625.7000	[J kg^-1]
Htotal	282981.0000	282952.0000	283045.0000	282930.0000	1.0003	92.9688	[J kg^-1]
Entropy	103.6010	104.8010	107.4800	107.4280	1.0256	2.6786	[J kg^-1 K^-1]
Mach	0.5330	0.5235	0.4486	0.4531	0.8569	-0.0749	
Cm	164.0090	173.6840	207.4760	208.2060	1.1946	33.7919	[m s^-1]
Cu	183.2610	168.6190	31.1099	30.3357	0.1845	-137.5090	[m s^-1]
C	250.9740	244.9750	211.9320	213.9150	0.8651	-33.0432	[m s^-1]
Distortion Parameter	1.0267	1.2141	1.1053	1.1059	0.9104	N/A	
Flow Angle	48.5595	45.3955	7.7113	7.2531	N/A	-37.6842	[degree]

The following table shows all the thermodynamic and aerodynamic properties of rotor 2 after the stall recovery. It can be seen from the data below that the compressor is counter-rotating since the flow angle alpha switches sign from positive to negative. All the parameters for the rotors are met. It can be noted here that outlet relative and absolute Mach numbers are slightly less than the design point numbers, this due to the fact that the increase in RPM causes stronger Shock and hence a decrease in outlet Mach numbers.

Table 3.15: Thermodynamic and Aerodynamic Properties for Rotor 2

Quantity	Inlet	LE Cut	TE Cut	Outlet	TE/LE	TE-LE	Units
Density	3.8299	3.7440	5.1589	5.1918	1.3779	N/A	[kg m^-3]
Pstatic	510917.0000	496266.0000	852626.0000	859980.0000	1.7181	356360.0000	[Pa]
Pt	607585.0000	613500.0000	1046490.0000	1032540.0000	1.7058	432986.0000	[Pa]
Pt (rot)	673144.0000	672899.0000	626165.0000	628908.0000	0.9305	-46734.1000	[Pa]
T	554.5260	551.3710	640.7900	643.3470	1.1622	89.4185	[K]
Tt	579.8010	580.8830	675.0690	674.5770	1.1621	94.1856	[K]
Tt (rot)	595.5230	595.8480	595.5590	595.6930	0.9995	-0.2885	[K]
H	257504.0000	254336.0000	344148.0000	346716.0000	1.3531	89812.0000	[J kg^-1]
Ht	282890.0000	283977.0000	378577.0000	378083.0000	1.3331	94600.0000	[J kg^-1]
Ht adiabatic	263135.0000	261982.0000	344438.0000	342683.0000	1.3147	82456.3000	[J kg^-1]
Ht polytropic	264360.0000	263371.0000	348664.0000	347022.0000	1.3238	85293.3000	[J kg^-1]
Rothalpy	298682.0000	299008.0000	298718.0000	298852.0000	0.9990	-289.7500	[J kg^-1]
Entropy	107.3950	111.2330	124.2150	126.4870	1.1167	12.9820	[J kg^-1 K^-1]
Mach (abs)	0.4534	0.5101	0.5182	0.4909	1.0157	0.0080	
Mach (rel)	1.1537	1.1810	0.6872	0.6933	0.5819	-0.4938	
U	472.9650	472.6570	472.6030	472.5760	0.9999	-0.0534	[m s^-1]
Cm	208.3330	226.8620	185.8100	180.6660	0.8190	-41.0520	[m s^-1]
Cu	29.9209	31.8672	-177.9350	-170.0560	-5.5836	-209.8020	[m s^-1]
C	214.1020	239.7330	263.8030	249.9460	1.1004	24.0695	[m s^-1]
Wu	502.8850	504.5240	294.6690	302.5200	0.5841	-209.8550	[m s^-1]
W	545.5950	554.1440	349.2450	352.9200	0.6302	-204.8990	[m s^-1]
Distortion Parameter	1.1033	1.0421	1.0288	1.0046	0.9872	N/A	
Flow Angle: Alpha	6.9392	7.7717	-43.0891	-43.2811	N/A	-50.8609	[degree]
Flow Angle: Beta	67.6190	65.7128	57.7835	59.2040	N/A	-7.9292	[degree]

Following are the contours for the compressor stages. It can be seen from the relative M contours for Rotor 1 that the shock is stronger than the design point due to the increased RPM of the rotor. Also, there is a shock induced separation at the trailing edge of the rotor at the suction surface. Fig below shows the relative Mach contours for the rotor. There are two shock located over the suction surface of this blade. The first shock is located at the leading edge of the blade and second shock is an ingested shock wave which results in boundary layer separation at the trailing edge.
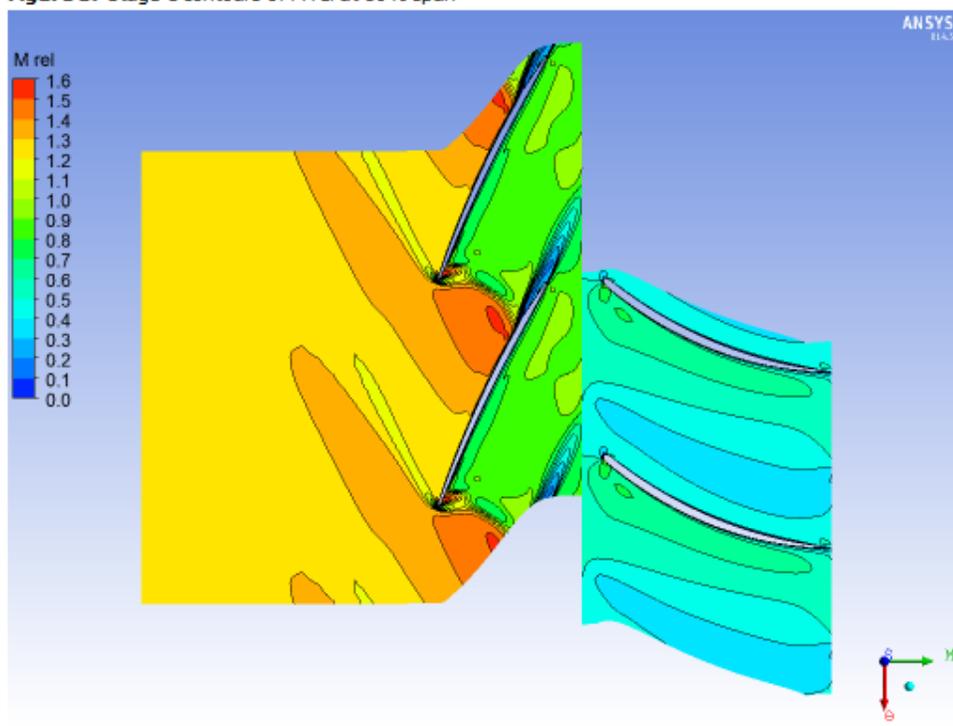
Fig 3.14: Relative Mach contours for Rotor 1
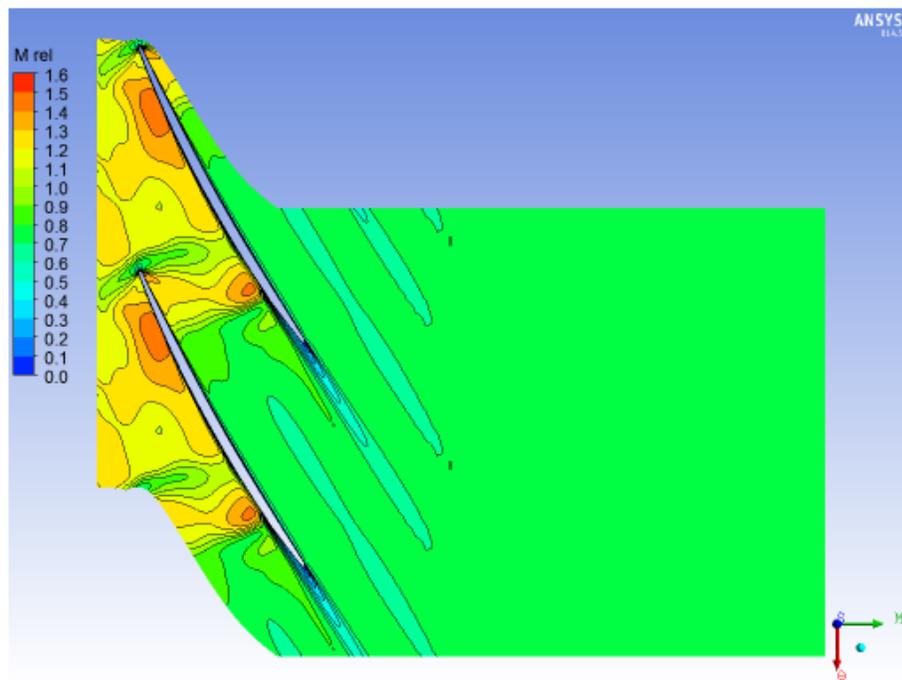

Fig 3.15: Relative Mach contours for Rotor 2
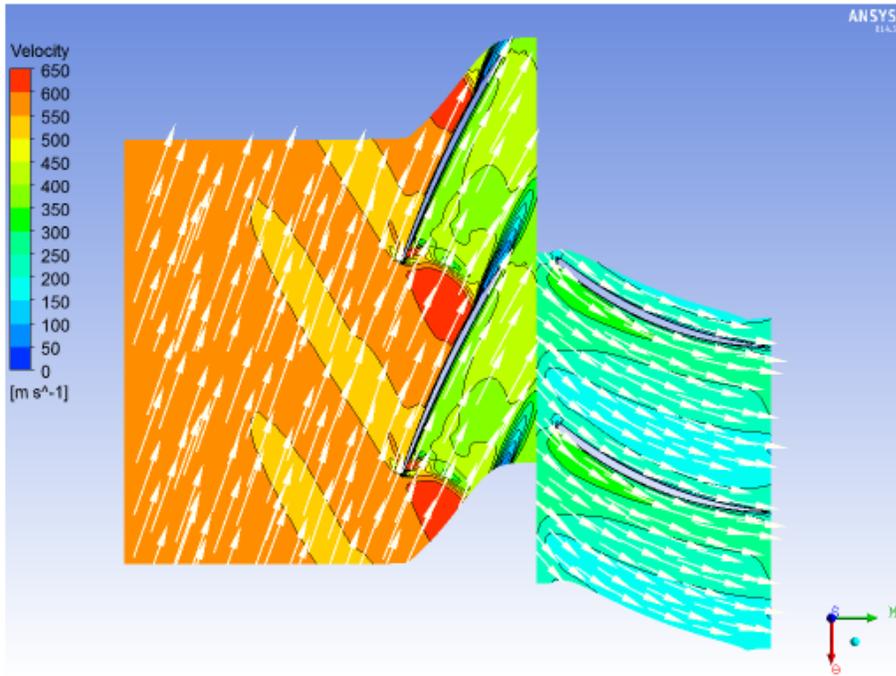
Fig 3.16: Relative Velocity Contours and Vectors for Rotor 1 and Stator 1 after stall mitigation
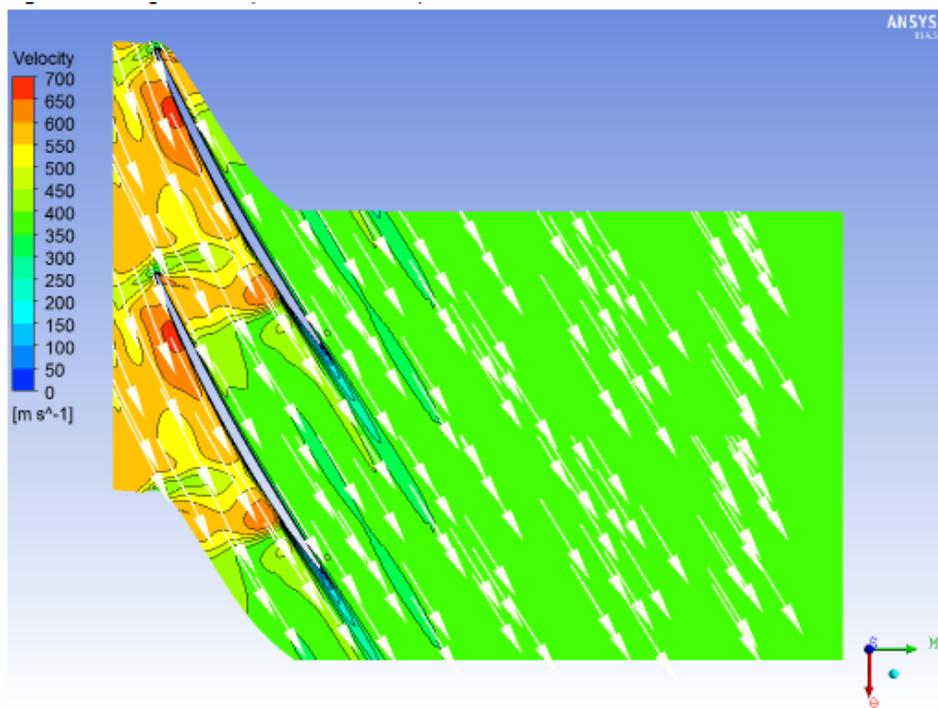
Fig 3.17: Relative Velocity Contours and Vectors for Rotor 2 after stall mitigation

The following charts show the inlet angles for Rotor 1 and Rotor 2. It can be seen from the charts that angles are not deviated along the span with an exception near the tip clearance.
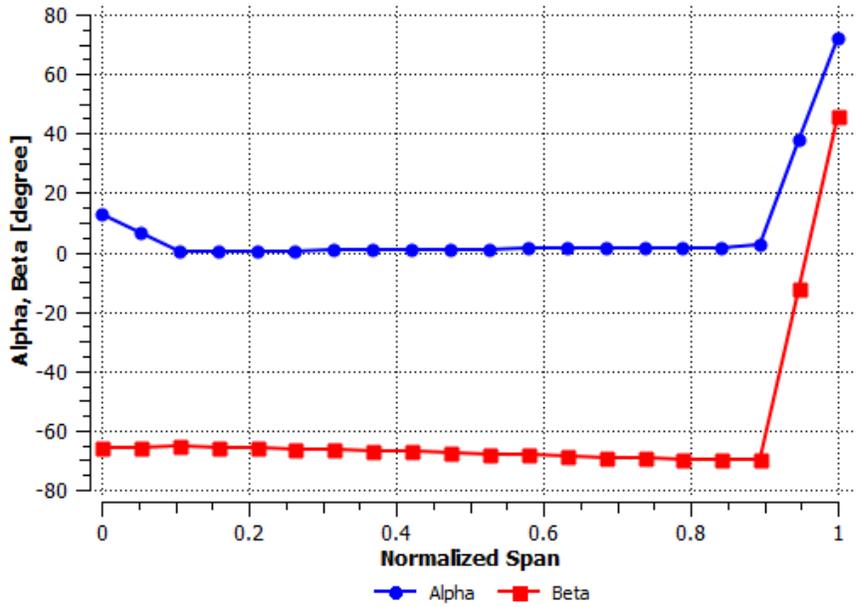

Figure 3.18: Rotor 1 inlet alpha and beta along the span
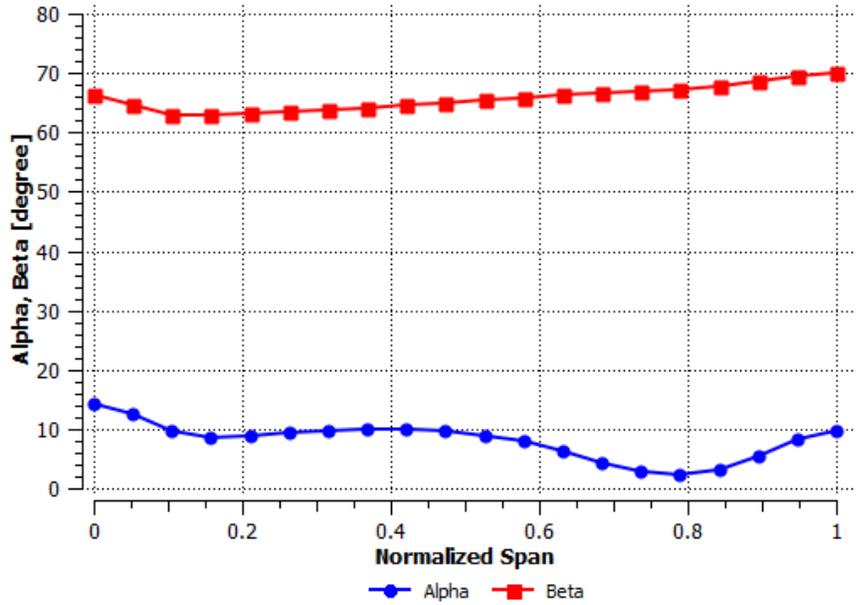
Fig 3.19: Rotor 2 inlet alpha and beta along the span

The following figures are Mach number blade loading charts along the stream wise direction. The plots give Mach number over the pressure and suction surfaces of the airfoil. The steep decline in Mach number suggests a shockwave.

It must be noted here that there is only shockwave that is induced at the leading edge of the blade. However, from the blade loading chart below it can be seen that there two shocks, one at the leading edge and another at the 75% of the stream wise location which could be due to the leading edge shock wave that propagates to the airfoil below it. (See Mach Contour, Fig below)
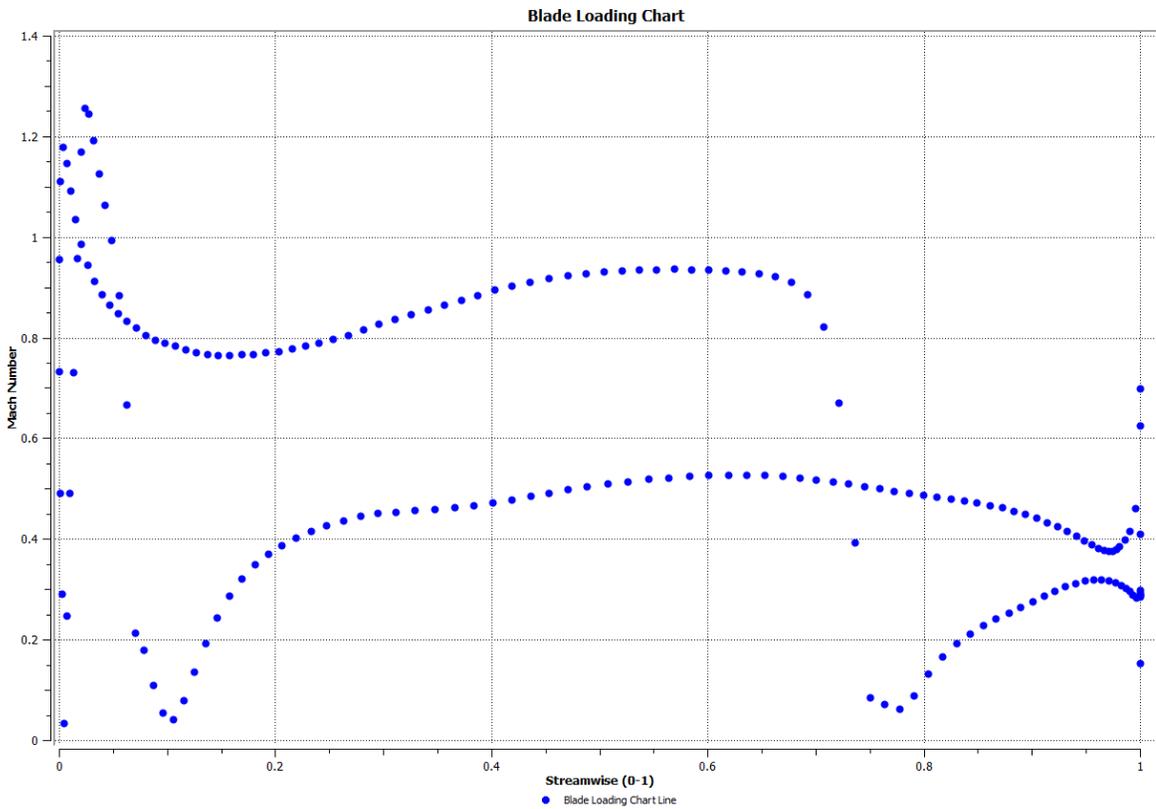

Fig 3.20: Mach number blade loading at 50% span for Rotor 1 after Stall Control
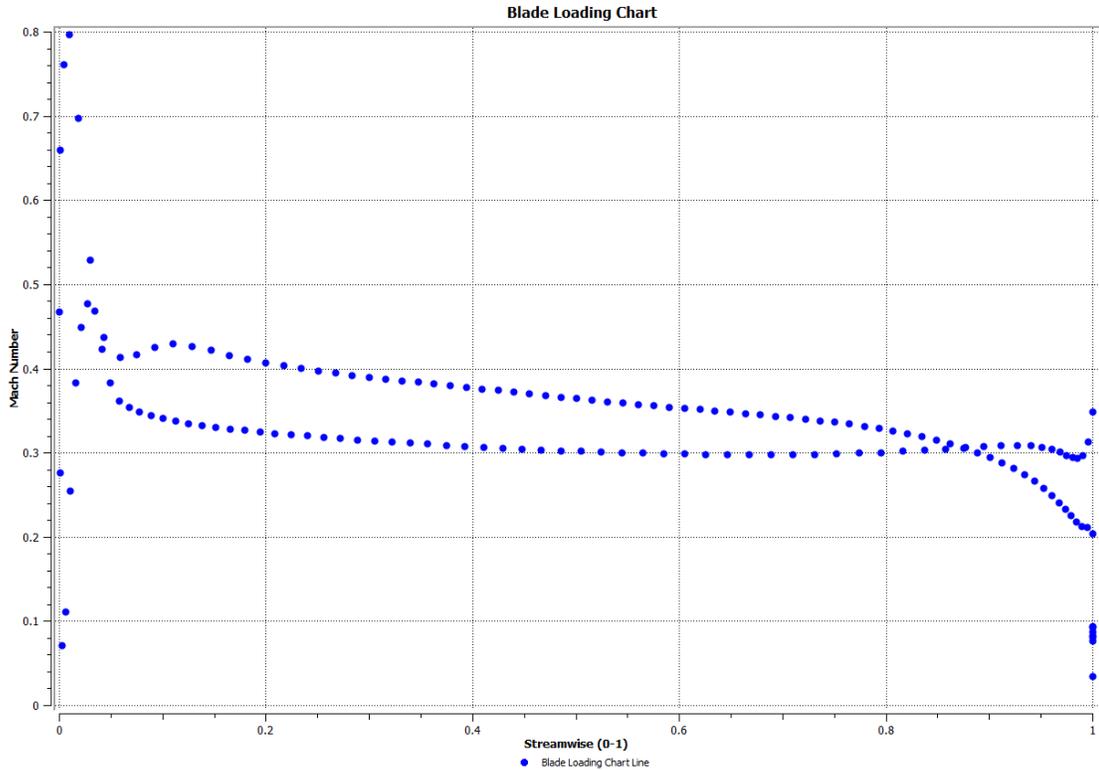
Fig 3.20: Mach number blade loading at 50% span for Stator 1 after Stall Control

The figure above shows the Mach number profile over the stator 1 at 50% of the span. It can be seen that the Mach number everywhere is < 1 suggesting that the flow is subsonic. The figure below shows Mach number blade profile of Rotor 2 at 50% span location. The flow is highly supersonic due to counter-rotating design which increases the relative Mach number at the inlet of Rotor 2.

Chart below shows the blade loading for Rotor 2. There are two individual shockwaves, one located at the leading edge and another at 80% of the stream wise location.
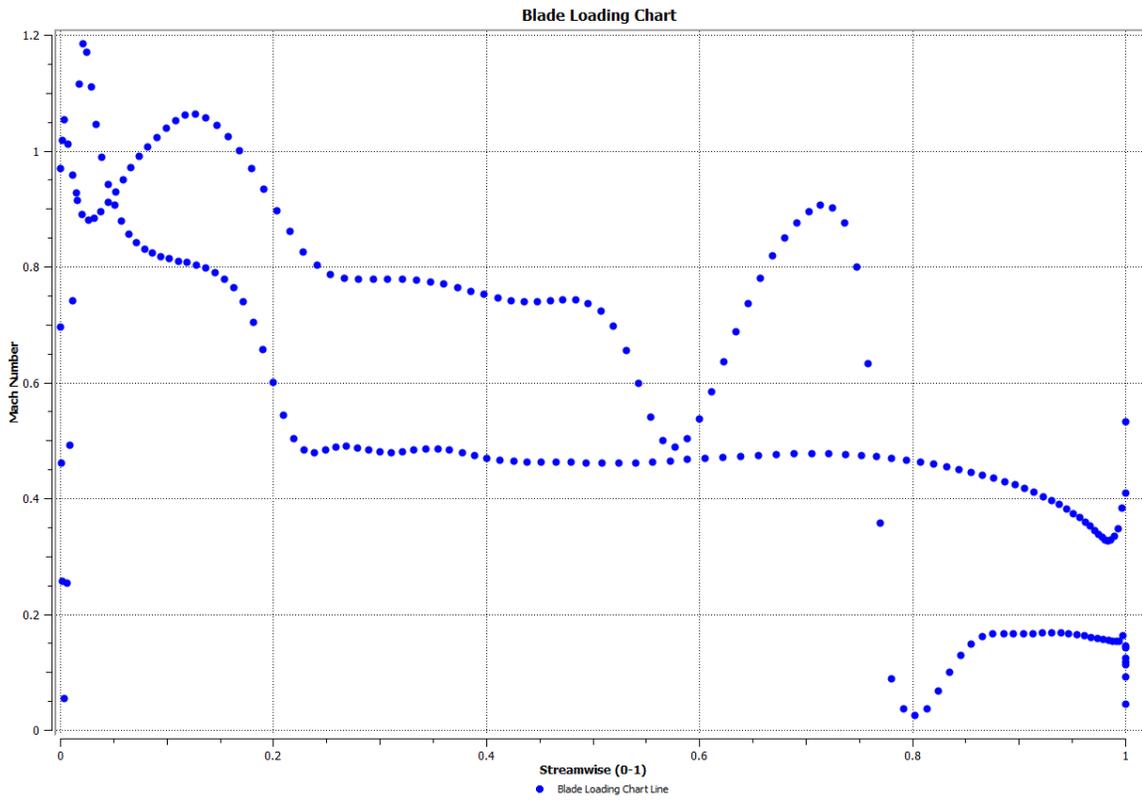
Fig 3.21: Mach number blade loading at 50% span for Rotor 2 after Stall Control

4.0 Conclusions and Recommendations

A novel computational study on an axial compressor has been performed to study stall and is mitigated by using counter-rotation and variable RPM spools in the compressor. Results have been presented on a number of flow parameters by the means of CFD post processing tools.

4.1 Conclusions

- Stall was successfully mitigated using counter-rotation and variable RPM spool. Increasing the RPM of the un-stalled rotor during stall helped to push in more mass flow and increased the overall velocity of the flow causing the separated flow in the compressor to reattach.

- The overall pressure ratio of the recovered compressor system was higher than design point compressor system as expected. This was due to the change in static back pressure at the compressor exit.

- During the compressor blade design it was seen that changing the thickness over the airfoil was seen to have a great impact on the shock wave placement on the airfoil. The number of shocks on Rotor 2 was reduced to 2 by decreasing the thickness of the blade. Leading edge radius was reduced and the shock wave became weaker. However, reducing the leading edge radius reduced tolerance of the rotor to change in incidence angles.

- Due to counter-rotation in the compressor, the work done by the rotors was high and hence higher pressure ratio was achieved. However, counter-rotation causes the inlet tip relative Mach number to increase and pushed the compressor design away from

design criteria. Therefore, it can be concluded that counter-rotation does not significantly increases the pressure ratio of the compressor due its design limitations. It can also be pointed out here that during this study an overall increase in RPM of both spools was also studied (i.e. RPM of both rotors was changed to 21000) to check if that corrects the stall in the compressor and the burden of using dual can be avoided. However it was found out that changing the RPM of the stalled rotor from 18000 to 2100 did help to alleviate stall, in fact it made it worse increasing the Mach relative tip number and casing more separation.

4.2 Recommendations for Future Work

- The present analysis indicated that change in thickness profile of the blades significantly affects the shock placements and susceptibility of the blades to change in incidence angles. Therefore, a thorough and robust design of the blades with detailed analysis on thickness profile is needed to be done in order to calculate the magnitude of the stall recovery system.

- Current analysis was done using a single passage in order keep the problem simplified. However, it would be very beneficial to preform CFD study using multiple passages in order to account for stall issues between passages.

- Stall is both a steady and transient phenomenon, in this analysis stall was treated as a steady state problem. Therefore, performing a transient type study would be beneficial in order to account for unsteady stall phenomena.

- In this analysis, the problem was kept to a 2-stage compressor design. However, in industrial applications axial compressors consists of multiple stages. A recommendation is made to study sequential counter rotation in multiple stages.

5.0 References

1. Giampaolo, Tony. *The Gas Turbine Handbook: Principles and Practices*. Lilburn, GA: Fairmont, 2003. Print.

2. Pampreen, R. C. *Compressor Surge and Stall*. Norwich, VT: Concepts ETI, 1993. Print.

3. Lorenzo, Carl F., Francis P. Chiaramonte, and Charles M. Mehalic. *Determination of Compressor In-stall Characteristics from Engine Surge Transients*. Washington, D.C.: National Aeronautics and Space Administration, 1984. Print.

4. Edwards, Phyliss. *Surge and Stall in Axial Flow Compressors, 1935-1973:*. Leicester (Cambridge Rd, Whetstone, and Leicester LE8 3LH): English Electric Ltd, Library, 1974. Print.

5. "Rotating Stall in Axial Flow Compressors." *Journal of the Aeronautical Sciences (Institute of the Aeronautical Sciences)* 24.11 (1957): 805-12. Web.

6. Day, I. J. "Active Suppression of Rotating Stall and Surge in Axial Compressors." *Journal of Turbomachinery* 115.1 (1993): 40. Web.

7. Sears, William R. "Rotating Stall in Axial Compressors." *Zeitschrift Für Angewandte Mathematik Und Physik ZAMP* 6.6 (1955): 429-55. Web.

8. Farokhi, Saeed. *Aircraft Propulsion*. Hoboken, NJ: John Wiley & Sons, 2009. Print.

9. El-Sayed, Ahmed F. *Aircraft Propulsion and Gas Turbine Engines*. Boca Raton: CRC, 2008. Print.